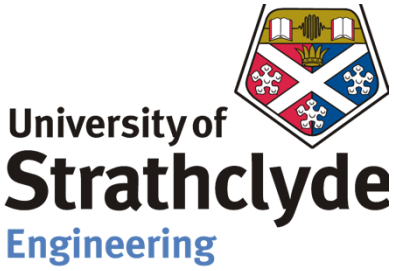

Department of Mechanical and Aerospace Engineering

Project

Inertial effects of multi-stream microfluidic configurations using simulations in Star CCM+

Author: Marc Bernal Martin

Supervisor: Konstantinos Zografos

A thesis submitted in partial fulfilment for the requirement of degree in

Master of Science in Sustainable Engineering: Renewable Energy Systems and the Environment

2021

Student No. 202076168

Copyright Declaration

Signed: Marc Bernal Martin Date: 30/8/2021

Student No. 202076168

Abstract

Shear-thinning fluids are numerically investigated using a model in Star CCM+ of a cross-slot configuration, imposing equal flow velocities at the inlet channels. The main technique used is a ramp down in generalised Reynolds number to investigate the effects on the central inertial instability during the steady-asymmetric flow above the critical conditions, and the transition towards a steady-symmetric flow below the critical conditions. The central vortex of the shear-thinning fluid results is numerically analysed and then compared with the Newtonian equivalent. The behaviour is characterised depending on the imposed generalised Reynolds number.

Student No. 202076168

Acknowledgements

This report could have not been completed without the support of the supervisor, Konstantinos Zografos, where regular orientation and advise was provided. Monica Oliveira also contributed to the completion of this report by providing additional support during these months. Their help is extremely appreciated, as this report could have not as detailed without their support.

Table of Contents

1.0 Introduction 10

2.0 Background Review 12

3.0 Problem description 25

4.0 Governing equations 28

5.0 Validation 31

5.1 2D straight channel, power-law fluids velocity profiles 31

5.2 3D straight channel, velocity profile 36

6.0 Numerical results 39

6.1 Results and discussion 40

6.1.1 N=1 40

6.1.2 N=0.8 44

6.1.3 N=0.6 47

6.2 Validation 50

6.3 Development velocity profile 53

7.0 Conclusion 54

8.0 References 55

9.0 Appendix 57

List of Figures

Figure 1- Front view of inlet channel A (Mesh scene) 25

Figure 2- Top view of cross-slot configuration..... 26

Figure 3- Numerical results of Star CCM+ vs analytical results of the velocity profile of fluid N=1 in a 2D channel 33

Figure 4- Numerical results of Star CCM+ vs analytical results of the velocity profile of fluid N=0.8 in a 2D channel 34

Figure 5- Numerical results of Star CCM+ vs analytical results of the velocity profile of fluid N=0.6 in a 2D channel 35

Figure 6- Comparison of the velocity profiles for the three different fluids in a 2D channel 36

Figure 7- Numerical results of Star CCM+ vs analytical results of the velocity profile of fluid N=1 in a 3D channel 38

Figure 8- Numerical results from Star CCM+ of the x-component velocity obtained from line probe 2 for fluid N=1 ramp down in generalised Reynolds number..... 42

Figure 9- Ramp down map depicting the maximum velocity of the central vortex for each different generalised Reynolds number for fluid N=1..... 43

Figure 10- Numerical results from Star CCM+ of the x-component velocity obtained from line probe 2 for fluid N=0.8 ramp down in generalised Reynolds number..... 45

Figure 11- Ramp down map depicting the maximum velocity of the central vortex for each different generalised Reynolds number for fluid N=0.8..... 46

Figure 12- Numerical results from Star CCM+ of the x-component velocity obtained from line probe 2 for fluid N=0.8 ramp down in generalised Reynolds number..... 48

Figure 13- Ramp down map depicting the maximum velocity of the central vortex for each different generalised Reynolds number for fluid N=0.6..... 49

Figure 14- Validation by comparing original mesh results with a more refined mesh results at Generalised Reynolds number of 50 for fluid N=1 51

Figure 15- Validation by comparing original mesh results with a more refined mesh results at Generalised Reynolds number of 75 for fluid N=0.8 52

Figure 16- Validation by comparing original mesh results with a more refined mesh results at Generalised Reynolds number of 75 for fluid N=0.6 52

Figure 17- Numerical results obtained from line probe 3 for the verification of the fully developed flow 53

List of Tables

Table 1- Numerical parameters used to determine the generalised Reynolds number and the imposed velocity required for the 2D channel validation 32

Table 2- Numerical parameters used to determine the generalised Reynolds number and the imposed velocity required for the 3D channel validation 36

Table 3- Numerical parameters used to determine the generalised Reynolds number and the imposed velocity required for the cross-slot geometry model with fluid N=1 41

Table 4- Characterisation of the behaviour of the flow depending on the generalised Reynolds number imposed for fluid N=1 43

Table 5- Numerical parameters used to determine the generalised Reynolds number and the imposed velocity required for the cross-slot geometry model with fluid N=0.8..... 44

Table 6- Characterisation of the behaviour of the flow depending on the generalised Reynolds number imposed for fluid N=0.8 46

Table 7- Numerical parameters used to determine the generalised Reynolds number and the imposed velocity required for the cross-slot geometry model with fluid N=0.6..... 47

Table 8- Characterisation of the behaviour of the flow depending on the generalised Reynolds number imposed for fluid N=0.6 49

Nomenclature

ρ	Density	Kg/m^3
U	Bulk flow velocity	m/s
Q	Volumetric flow rate	m^3/s
n	Power law index	-
H	Heght	m
u/U	Dimensionless velocity	-

1.0 Introduction

The development in rheology and microfluidics in the last few decades has led to a great number of improvements in different fields, ranging from industrial, medical to engineering. The more understanding that is acquired through investigation about different configurations and different types of fluid, the bigger the capacity is to exploit these rheological behaviours and range of operations, which can later be extrapolated and implemented in an extensive range of applications.

This paper is a numerical investigation of the effects of different fluids on the inertial flow instability that occurs in a cross-slot configuration. A systematic review of existing literature is done, starting from the basic principles and goals of rheology and microfluidics, to discussing different investigations in 2D planar mesh and 3D volume mesh published articles and ending in a detailed review on past work performed on cross-slots. There exists an enormous body of literature regarding Newtonian fluids, but not as much has been characterised for non-Newtonian fluids. The results of this investigation will aim to fill some gaps in the literature of shear-thinning fluids.

This investigation will use the Power law model to model shear-thinning fluids in a cross-slot configuration. Star CCM+ was used as a computational fluid dynamics simulator. A process of validation was performed comparing analytical results obtained from equations with the results extracted from Star CCM+ for a 2D straight channel with different power law fluids, and a simple Newtonian fluid in a 3D straight channel. This step gives a certain level of confidence in the results that will be obtained from the investigation, establishing that the model works in the way it is supposed to.

The main body of the investigation focuses on the numerical analysis of an inertial flow instability using computational fluid dynamics to simulate shear-thinning fluids in a cross-slot configuration. The simulations for each different fluid are started by imposing a high generalised Reynolds number, well above the critical value, and perform a ramp down process. The aim is to observe the transition from steady-asymmetric flow to steady-symmetric. These results are then compared to the equivalent Newtonian fluid to characterise any differences. The focus of this study is

on the central inertial flow instability that occurs at the intersection of the geometry, where the stagnation point occurs. This is the most distinguishing characteristic of the configuration used. The results from the investigation will be presented in a dimensionless manner so the data is easier to extract and extrapolate for other uses.

2.0 Background Review

Rheology is the term that describes the science of flow of matter and deformation. This independent branch of science is relatively new, having emerged less than a century ago. This term was invented in 1929 by E.C. Bingham and his Lafayette College associates [1]. This science came to be from the observations of abnormal behaviour of fluids, or non-Newtonian as we know it today, in popular materials such as paint, clay, oil… Paint is meant to be a liquid but when applied to the wall it adheres without sagging down, which would not happen with water. The modern concepts of liquid and gas are also essentially models which were mathematically represented by the efforts of Robert Hooke and Isaac Newton [2]. When research into this kind of abnormal materials began, the term solids and liquids were found to not be enough to describe their properties, due to the fact that some of these non-Newtonian fluids had both liquid-like and solid-like properties.

All of the natural sciences attempt to deal and understand reality with the use of phenomenological models. This is a scientific model that empirically describes the relationship of phenomena to each other. Any model is used as a tool to understand not all, but the most significant characteristic features of the material under investigation.

In rheology there is a first main goal, which is to investigate and establish the relationship that happens between applied forces and geometrical effects caused by such forces at a point of interest. The next independent goal of this science would consist of developing relationships between the molecular composition and the rheological properties of a material.

By common approval, rheology is known to be a difficult field. This is surely the most common first impression a newcomer would have. As stated in the book “An introduction to rheology”, due to the interdisciplinary nature of the subject, most of the engineers and scientists who join are forced to move away from a normally restricted area of expertise and have to develop a much broader scientific approach [3].

Rheology, as mentioned above, is a multidisciplinary science which has its main relationship with chemistry and physics. The link with physics is that both are based on predictions and explanations of rheological properties through fundamental laws of physics and knowledge of molecular structure. On the other hand, rheology's connection to chemistry can be expressed by existing experimental proof of direct correlation between rheological properties and chemical parameters [2]. Individuals who work in rheology must become comfortable with specific well-defined sub-areas. These would be rheometry, constitutive equations, calculations of the behaviour in complex flows and the measurements of behaviour of the flow in complex geometries [3].

The main theoretical concepts are kinematics, conservation laws and constitutive relations. Kinematics addresses the geometrical aspects of deformation and flow. Conservation laws deal with stresses, forces and energy interchange. Constitutive relations are used to relate the forces and motion in order to complete the description of the flow processes. This may then be used to solve engineering problems, as this paper will do. Constitutive equations, also known as rheological equations of state, are equations that relate appropriately defined deformation and stress variables. These can be derived from a microrheological perspective, in which the molecular structure is considered principally. A different approach is to have the macroscopic perspective, also known continuum. This way the individual microscopic behaviours are not directly addressed.

All materials in the real world possess a microstructure at the molecular, crystal, or further level. In mechanics we do not normally consider the discrete nature of matter. The area of interest usually resides in the large-scale phenomena which involves the average behaviour of a very large number of units of the microstructure. Continuum mechanics studies the mechanical behaviour of solids and fluids at a macroscopic level. It is the mathematical study of the response of these ideal bodies to deformations and applied forces [4].

As previously mentioned, rheology appeared from the study of abnormal fluids. Newtonian fluids are simple and behaved in expected ways, as can be described by the Navier-stokes equation [5]. This equation cannot be applied to non-Newtonian fluids due to their complex structure. Some of these non-Newtonian or rheological effects which have been studied are Shear-rate dependent viscosity, Normal-stress

effects in steady flows and Transient responses in unsteady shear flows. In this paper, the focus will be on Shear-rate dependent viscosity.

Shear-rate dependent viscosity means that their viscosity is correlated on shear rate or the deformation history. For the dependency on the shear rate there would be shear-thickening, in which the viscosity increases with increasing shear rate, while shear-thinning- on the other hand, its viscosity decreases with increasing shear rate. Viscosity is normally the most important parameter in engineering applications. Fluids that depend on deformation history are called Thixotropic fluids. This behaviour can be defined with the following equation:

Eq 1 $\tau=\eta U/d=\eta\dot{\gamma}$

The shear stress (τ) is related to the shear rate ($\dot{\gamma}$) by the shear viscosity (η), while U is the velocity and d the distance of the velocity profile [1].

Another behaviour of these materials in shear is the time-independent non-Newtonian fluids. When the structural changes with time are ignored, there is a possible model for inelastic, non-Newtonian fluids given by this equation:

Eq 2 $du/dy=\dot{\gamma}=f(\tau)$

The equation above suggests that the shear rate ($\dot{\gamma}$) at any location in a fluid is a function of the shear stress (τ) at that same point. These models for fluids can be called non-Newtonian viscous fluids or generalized Newtonian fluids. By developing such models, they give us the chance of predicting the behaviour of these fluids and even take advantage of certain properties. These fluids can be divided into three groups, depending on the nature of the previous equation. These are Bingham plastics, pseudo-plastics (shear-thinning fluids) and dilatants (shear-thickening fluids) [1].

As discussed, models are tools to characterise the most important characteristic features of the matter to be studied. Having the capability to accurately characterize and analyse non-Newtonian fluids is a vital skill when it comes to the manipulation

and distribution of these fluids. This topic of research has been going on for decades having developed numerous different models addressing different features at different levels of complexity to achieve their analysis. A simple model, which will be the one used in this paper, is the Power-law model. This model is also known as the Ostwald de Waele relationship. This model is described by the equation below:

Eq3 $\eta = K\dot{\gamma}^{(n-1)}$

Where η is the viscosity, n is the power law constant and K is the flow consistency index. This model is used to place non-Newtonian data along shear rates where there is no indication of a Newtonian Plateau [6]. The power-law model is one of the most famous models due to its simplicity, having only two fitting parameters, while other models used for similar cases such as the Carreau-Yasuda model or Cross model have up to 4 or 5 fitting parameters, making them much more complex.

The power-law constant (or flow behaviour index) will be used to classify the fluids to be simulated. Based on the power-law index (n), if $n<1$ the fluid will exhibit shear-thinning (or pseudo-plastic) behaviour. The smaller the value the higher the degree of shear-thinning characteristics. If $n=1$, the fluid has Newtonian behaviour. If $n>1$, the fluid exhibits shear-thickening (or dilatant) characteristics, increasing with increasing index value.

In the last century technology has been developed at an exponential rate, giving access to fields of investigation that were not even considered previously. An example of these is the field of miniaturization. In the last decades, a significant amount of progress has been achieved, making it now possible to miniaturize all type of systems. Some examples of this could be fluidic, mechanical or even electromechanical up to sub-metric sizes. Less than half a century ago, in the 1980s, the progress made in miniaturization gave birth to a new field which is called MEMS (microelectron-mechanical systems. Once the potential of this was acknowledged, this field diversified into all kind of applications such as biological, chemical or biomedicine. The way these systems worked was by employing flows working under unknown and strange conditions. This led to the rise of a new field called microfluidics [7].

A simple way to define microfluidics is the study of the flows which are circulating in an artificial microsystem. Its both the science which studies and analyses the characteristics of these fluids, and at the same time manufacturing technology which creates miniaturized devices with different geometric configurations.

The first devices in this field appeared at the end on the1980s in two different places. At IBM in 1977, ink jet printer nozzles were in the process of development. This set of uniform nozzle arrays was a crucial part of actually implementing high speed and high resolution ink jet printing [8]. Stanford University was performing research involving a gas chromatograph system in 1979 [9]. This impressive device worked by circulating gas through microchannels made in silicon. It was based on a miniaturized thermal detection and a miniaturized electromagnetic injection. All this was within a single chip which only measured a few centimetres in width. Only about 20 years later, people realised the numerous advantages of microfluidics, which made this field gain the spotlight. After that moment, all kind of microfluidic systems began to be manufactured, such as the electroosmotic pumping system, micromixers, DNA amplifiers, chemical microreactors and many more [10]. This enabled a whole new level of precision and efficiency to be added to many different fields.

Two main ways of simulating fluids exist. These are 2D and 3D. However, like most things, there are advantages and disadvantages to both types. To begin, 2D flows are not real, in the way that they do not exist in nature. Some configurations are similar to this, such as flow over a plate, but they will lack some key characteristics only present in 3D. Also, 2D can give us useful approximations such as aerofoil analysis in aerodynamics. When comparing fluids simulated with a planar mesh (2D) and a volume mesh (3D), sometimes the differences can be predicted. In the case of a flow-mixing configuration, if the volume mesh cross-section is rectangular, it will have a similar result than the planar mesh. Most of the phenomena in fluids are never purely 2D. 2D simulations will run significantly quicker than their 3D counterpart. This is because as there is a whole less dimension, this will reduce the individual points to evaluate, reducing the number of equations required for the simulation. This can be explained by the square-cube power law [11], the scale of the problems depending on the resolution of the mesh chosen go up by a factor of L^2 . When you perform a 3D model, the scale of the problems go up in a scale of L^3.

When reviewing planar mesh investigations, a popular tendency can be observed that inclines studies towards analysing certain characteristics of fluids. These can be wall-effects, different configurations, drag coefficients and the effects of variations of blockage ratio and flow patterns on different types of fluids. The fluids of interest will be Newtonian, Shear-thinning, or Shear-thickening.

It would be no surprise if the amount of literature on the subject of bluff body wakes that has been developed since the start of early last century would impress any newcomer. The fact that so much investigation has been focused on this field just shows both the difficulty of first understanding, and then describing appropriately the flow behaviour under different conditions that would occur in a viscous flow. Even flows which have a relative simple configuration, like those past a cylinder, have managed to attract the interest of scientists from different fields into the array, which after decades has only just recently started to reach consensus on the matter. This is an attestation of the complexity of the subject.

In a paper published in 2004 [12] the existing literature is commented upon. It can be seen that some simple effects of varying the blockage ratio have already been described. One would be that in the steady flow regime, if the blockage ratio is increased by bring the walls closer together whilst maintaining the dimensions of the cylinder derived in the emergence of twin vortices in the region of the cylinder wake, happening at high Reynolds number. Another effect described is that at any Reynolds value lower than 50, and for a blockage ratio smaller than 0.2, the closed vortex bubble decreases in length with wall proximity. When performing experimental and numerical investigations, bounded domains give a more definite specification of the rheological behaviour of the flow, than in the unbounded cases. This paper performed a velocity-only numerical investigation of the effect the walls would have when increasing blockage ratios in a two-dimensional flow past a cylinder. They focused on investigating this effect on certain properties, these were stability, wake structure, hydrodynamic forces and Strouhal number [13]. One of the behaviours they found showed that for Reynold's value under 280 and a blockage ratio of 0.9, there was (minimum) three individual curves of neutral stability.

An article released in 2007 investigated the behaviour of drag coefficient and wall effects on power-law fluids across a circular cylinder in a confined channel [14]. As stated in the paper, due to previous efforts in the field, an extensive amount of information on transverse flows over a circular cylinder in an unconfined configuration exists. On the other hand, there is a lot less known about the effect of including confining walls on the flow behaviour, even for simple fluids. This is one example of the stage at which this field is at, having a lot to be analysed still. A significant wide variety of different conditions were computed, these were the Reynolds number (between 1-40), power-law index (between 0.2-1.9, therefore covering shear-thinning, Newtonian and shear-thickening) and the blockage ratio (between 4-1.1). Many extremely useful and applicable results were obtained for different properties, like drag phenomena (pressure drag coefficient, friction drag coefficient, total drag coefficient, and drag ratio), detailed flow characteristics (streamline patterns, surface pressure coefficient). They observed that independently of the blockage ratio between the cylinder and the walls (β), there was an improvement in the drag coefficient when the shear-thickening tendency of the fluid increased. Conversely, the shear-thinning exhibited the opposite dependence. Another characteristic observed was that the confining walls apparently delayed the separation of the flow in the case of shear-thickening fluids, while the opposite behaviour was observed for shear-thinning fluids. The behaviour of power-law fluids was computed, observed and analysed in order to improve our understanding of these complex fluids. This research has an extensive range of applications in the real world. Some of these examples could be pin or tubular heat exchangers [15], where more understanding of the behaviour of flow around certain geometries and the heat-exchange occurring under certain conditions may enable us to develop much more efficient heat exchangers.

The more knowledge is acquired in this field, the more apparent it is that there is so much more to study by performing similar investigations but under different conditions and parameters due to the complexity of some rheological behaviours. An article which was published in2019 in a journal of applied mathematical modelling [16] shows that the level of investigations is evolving to be much more complex and is carried out over a wider array of conditions. This numerical study was done again on the effects of the blockage ratio but was performed under one cylinder and two cylinders in tandem, confined, and unconfined, 2D and 3D. Even further, different

power law fluids were implemented adding to the complexity. The rheological behaviour on the flow movement of the different fluids was numerically studied. This particular arrangement, when contemplated about in the physical point of view, the case of the tandem cylinder configuration is related to a wide range of variables that define the rheological behaviour. Some of these variables are the number of cylinders implemented, the distance between these and the influence of different Reynolds number. The power-law model was used as a constitutive model in order to observe correlations that could be extrapolated to other fluids with a higher level of complexity. One of the applications of this specific study could be to utilise these rheological behaviours as the basic principle for an innovative design which could promote different mixing capacities by changing the working fluid used [17]. This type of approach has proven really useful, shown in the conclusions of this paper. Some of them are that shear-thickening fluids have a higher critical Reynolds number when comparing it to shear-thinning fluids in confined cases of both one and two cylinders. On the other hand, it was also concluded that shear-thickening fluids have a lower critical Reynolds number than shear-thinning for the unconfined cases. Many more conclusions about the effects the addition of another cylinder, increased confinement and 3D cases were described.

The set of literature for flows around cylinders is significantly extensive, owing that to the extensive range of applications this geometric configuration has. Heat exchangers is one of the most popular applications, where more knowledge of the interaction between the geometry and the fluid could lead to devices with significantly increased efficiency. Some of the applications can also be on a large scale, such as with offshore wind farms, where the underwater structure tends to have circular cross-sections and one of the most important requirements for this case is stability and robustness [18]. Also adding that lower drag would lead to less erosion and decay of the components, leading to cheaper maintenance.

Non-Newtonian fluids are also crucial for a wide spectrum of scientific fields. Some engineering applications could be polymer and food industries, due to the non-Newtonian nature of many of the fluids manipulated. Biomedical engineering and medicine also benefit from increasing knowledge of the rheological behaviour of non-Newtonian fluids because of the complex body fluids, such as blood [19]. All the knowledge obtained from studies and investigations can be extrapolated into numerous different fields with alternative operating conditions and geometries.

An alternative type of configuration for a 2D planar mesh could be of a sudden expansion. In 2013, a journal was published on a numerical investigation that was performed in a 1:3 ratio planar sudden expansion for power-law fluids [20]. The aim of this experiment was to investigate the rheological behaviour of power-law fluids when encountered by a sudden expansion. In the case of a Newtonian fluid, as the literature already exists, at a low/moderate Reynolds number when it encounters a sudden expansion in a 2D channel, flow separation occurs creating a pair of symmetric recirculating eddies along the walls going downstream. If the Reynolds number was increased above a certain critical value, the vortices will evolve into steady-asymmetric. The Reynolds was increased even further in the hope of finding some rheological phenomena, which did happen when a third vortex was formed downstream of the two vortices mentioned previously. The range of power-law fluids that was analysed went from 0.2-4, giving the properties for Newtonian, shear-thinning, and shear-thickening. In addition, in this journal the Generalised Reynolds number was utilised instead of the conventional Reynolds number, which will also be used in this paper later. Some of the conclusions brought in the journal are quite interesting. One being that the bifurcation in the flow is delayed in the presence of a shear-thinning fluid when compared with the Newtonian. As expected, for the shear-thickening fluid the behaviour was seen earlier than for the Newtonian. The characteristics of the recirculating eddies at the walls also changed, making them more elongated as the shear-thickening behaviour was intensified. For the shear-thinning, they became more curved the more shear-thinning the fluid was.

Using 3D volume meshes, as mentioned before, has different implications to the previous 2D examples discussed. When using 3D meshes the level of complexity evolves significantly, but so also do the possibilities of configurations and rheological behaviours. In this field, as seen in the literature, different fluids are investigated but are not as focused on configurations such as flow over cylinders, the interest being in completely different geometric configurations. Two of the most popular and useful properties of 3D investigations is the ability to mix two fluid flows and the manipulation of particles on the micro and nanoscales. Deriving from the increased use of microfluidic devices across many fields, such as biomedical diagnostics and chemical fields, the ability to manipulate a particle or mix two fluids has become an extremely tempting field of research. These devices are usually needed in a really small scale, and because of this, the inertial forces are normally

small, therefore laminar flow is predominant. This behaviour makes the process of mixing fluids rely on molecular diffusion. This is significantly inefficient when compared to turbulent convective mixing. Some of these can be a T-shaped, H-geometry and cross-slot. A review of previous work using these configurations will be done observing the different characteristics of each configuration as well as the potential applications these could have.

The T-geometry is widely popular due to its simplicity and applicability. It is established that above a certain Reynolds number (dependent on aspect ratio), the flow can break symmetry inside a 3D T-channel. This phenomenon has been used as a method of improving mixing in microfluidic channels. When investigated, it has been shown to produce significant increases in mixing quality beyond the bifurcation and the intersection. The geometry consists of two-square inlets and an outlet which has an equal combined area. The two inlet opposing channels join at the intersection turning 90 degrees. It was found out that the resulting flow in this configuration in the outlet channel can be characterized by three flow regions within the steady flow. These would be “vortex” flow, “stratified” flow and “engulfment” flow [21].

A journal in Chemical Engineering Science investigated the effects of shear-thinning and aspect ratio on this configuration [22]. The investigation consisted of exploring the critical conditions which derived in the steady symmetry-breaking phenomenon. This was done by varying the aspect ratio of both inlet channels over a considerably wide range. It was possile to show that the change in flow behaviour, going from symmetric to asymmetric was (in most cases) a steady supercritical pitchfork bifurcation. It was confirmed than an existing relation for attempting to predict the critical conditions can fail to work under specific combinations of aspect ratios.

The H-geometry configuration is a bit harder to understand than the T-geometry. It is made up of two straight square parallel channels where the flow of the fluid enters the channels in opposite directions. It has a central gap between the channels that allows both flows to interact. When the conditions are under creeping-flow, the flow seems steady planar and exhibits a sharp interface between the two flows. When the Reynolds number goes over certain critical value, one out of two possible behaviours may occur. These would be supercritical inertial instabilities which alter the flow pattern significantly. This produces the two flows to interact much more while remaining steady. The behaviour of the instability can be altered by varying the size

of the gap between the channels or by varying the Reynolds number. Two instabilities were identified, one of them appears in configurations with a relatively small gap size, while the other appears with big gaps. When using a value in between these two gaps both instabilities will appear at the same time [23]. Having the ability to control the combining and separation of fluid flows in a microscale has a vast range of applications within the industrial, scientific, and medical fields.

Cross-slots have recently become popular within the extensional flow configurations. This is thanks to the ability to enable a variety of different operations and geometrical simplicity.

A cross-slot geometry is composed of 4 intersecting channels. Two of which are opposing inlets and the other two are opposing outlets. The two inlets have a particular fluid flow which is imposed to be at the same flow rate, where they meet at the centre of the configuration and interact. When they meet, a stagnation point is generated at the centre. This characteristic is the trademark characteristic of this configuration. For small Reynold's value (below critical), the flow remains steady-symmetric and could be seen as an almost 2D flow. When the Reynolds number is increased above the critical value the behaviour of the flow changes dramatically, a single-spiral vortex is created, and the flow evolves a bifurcation to a steady-asymmetric state. From this state at the intersection, an axially-aligned spiral vortex extends through the outlet channels

The ability of creating a stagnation point without the need of an obstacle like a sphere is an extremely useful property in a lot of fields. The most important property of these stagnation point flows is that fluid "particles" are stuck at the stagnation point and are put through high strain rates for finite time, or they are put through high velocity gradients at the area around the stagnation point for limited time too. The significance of stagnation point flows was firstly addressed by Taylor, who in 1934 created the four-roll mill design. The device consisted of a square container with a hole through which fluid was added. This square device contained four cylinders at each corner, powered by shafts linked to a pair of cylinders, which rotated at equal speeds but in opposite directions thus creating a specific flow with a stagnation point at the centre of the configuration [24]. This device enabled Taylor to create powerful extensional flows using a matrix fluid and further deformations. It could even provoke the break-up of particular droplets by catching them in the stagnation point.

The cross-slot configuration can be seen as a fundamental base-case geometry. It represents a stagnation point and planar intersecting forming flow geometry. The more that is understood about the behaviour of flow in this geometry and as the body of literature grows, the more applications of fluidic systems this configuration could be utilised for.

An article published in 2016 investigated the fluid flow within a cross-slot configuration while varying the depth to width ratios [25]. The creation of vortices with a Reynolds value over a moderate one in the configuration was analysed. The difference in the pattern of the flow was compared with the Taylor vortex formation, while demonstrating that it is due to extensional flow in the vicinity of the stagnation point instead of by centrifugal effects. One of the observations done was when using a deep cross-slot cross-sections, the instability takes the shape of a pile of 3D spiral structures that can be seen in the central intersecting region. It was also demonstrated for a flow with a Reynolds value above the critical value in cross-slot configurations, that the steady spiral vortex instability seen is well expressed by a Landau model. New information found performing these investigations can be implemented in many different fields. Many areas of research, such as viscoelastic fluid properties and macromolecular dynamics [26] [27]. It can also be used to control deformations in particles [28]. Only recently, it was also shown that a microscale device utilised the flow instability within the cross-slot promoted mechanical scission of polymer chains [29].

Another approach in investigations using the cross-slot device can also be varying the working fluid, instead of changing the dimensions as in the example above. The same journal published an article addressing this in 2017. The investigation consisted of studying the effect of adding quantities of a flexible polymer into the working fluid, in this case a Newtonian solvent [30]. It was shown that by doing this mixture, there was a significant effect on the onset conditions for the flow instability, and therefore the growth of the axially aligned vortex. This investigation facilitates the study of these interactions between the inertial flow instability and the altered elasticity properties. It was seen that while slowly increasing the elasticity properties, the flow was destabilised at a significantly small critical Reynolds value than for the simple Newtonian example. This investigation approach can be used in industrial applications by extrapolating the knowledge acquired and implementing it in industrial properties with similar working conditions.

A more recent article released in the journal of non-Newtonian fluid mechanics numerically investigates the behaviour and effects of viscoelastic fluids in a 3D cross-slot device [31]. The shape of the channels used for this study was square cross-section, having an aspect ratio of 1, maintaining it at that value throughout the investigation. This study focuses on the effect on the inertial instability above certain critical Reynolds number which leads to a steady-asymmetric flow. The results released here show how utilizing different models for viscoelastic fluids will have an impact on the behaviour of the instability in the central region of the configuration. All the models used showed a common rheological behaviour, changing the onset critical conditions for the flow asymmetry. All the data demonstrated the critical Reynolds value was lower compared to a Newtonian fluid, both for decreasing and increasing ramps. The results also showed a hysteric behaviour between both ramps for the critical conditions of the flow transition, which also happened for the Newtonian fluid.

As seen by the extensive existing literature related to cross-slots, due to the properties of the configuration, it has countless fields where it could be used. Cross-slots can be used in experimental techniques due to its planar nature. This permits the behaviour of complex fluids subject to extensional flow regions in order to be understood and characterized. Another use of cross-slots could be rheometers, due to its ability to manipulate particles enabling large deformations around the stagnation point to be done [32]. The field of biomedical research would also benefit from this configuration, individual cells could be trapped within the stagnation point and analysed in detail, enabling manipulation of individual particles, such as DNA molecules [33]. As previously discussed, microfluidic device flow tend to reside in the laminar regime, which makes mixing a complicated task. The instabilities and non-linearities could be utilised as an advantage to enhance mixing qualities. The characteristic of the spiral vortex could also be used to enhance heat-transfer ([34], offering an effective alternative instead of modifying the geometry or requiring external forcing.

3.0 Problem description

In this investigation a cross-slot device was used to exploit the inertial flow instability phenomenon of this configuration and an analysis was performed on the behaviour of Newtonian and Shear-thinning working fluids. The computational fluid dynamics software (Star CCM+) used to achieve the study was initially validated using a 2D planar mesh channel and 3D volume mesh channel with analytical equations in order to validate the accuracy of the software. Once this was completed, a cross-slot configuration was created.
The device used in this experiment is made by mutually bisecting channels. These square-channels can be seen in Figure 1, measuring 1m x 1m and being of constant height and width.

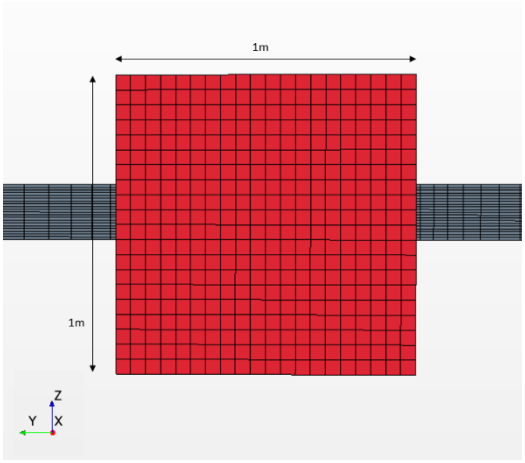

Figure 1- Front view of inlet channel A (Mesh scene)

In figure 2, a top view of the configuration can be seen. The horizontal channels (aligned with the x-axis) are the two inlets, flowing in equal but opposite directions towards the centre. The inlet channels have a length of 20 metres, long enough to allow the fluid velocity profile to be fully developed. This development was also verified using a line probe (line probe 3) along the inlets. This would make any rheological behaviour of the flow in the intersection and after be due to the inertial instability created by the device. The two vertical channels (aligned with the y-axis) are the outlets, where the axially aligned vortex flows and dissipates. In order to create a nicely refined mesh for the device, 5 different bodies were created, these being the two inlet channels, two outlet channels and the centre cube where the intersection occurs. The flow was initially imposed at a predetermined velocity at the velocity inlet in the inlet channels. This fully developed flow then meets in the centre cube where it interacts and is released through the two outlet channels towards the pressure outlet. A directed mesh was utilised with a base size of 0.05m, as seen in Figure 1. As the centre and outlet channels are linked to the inlet channels, once the

mesh is modified in the inlet channels the base size of the other three connected bodies is modified automatically to match. A one-sided geometric stretching function was utilised for both the inlet channels and the outlet channels, concentrated towards the centre so there was a higher resolution in the region of interest. Both sets of channels had different values for the function to achieve a refined mesh. The inlet channels had 40 layers and a stretch value of 1.12, while the outlet channels had 45 layers and a stretch value of 1.1, to create a nice transition of the meshes between the bodies, as shown in Appendix 1.

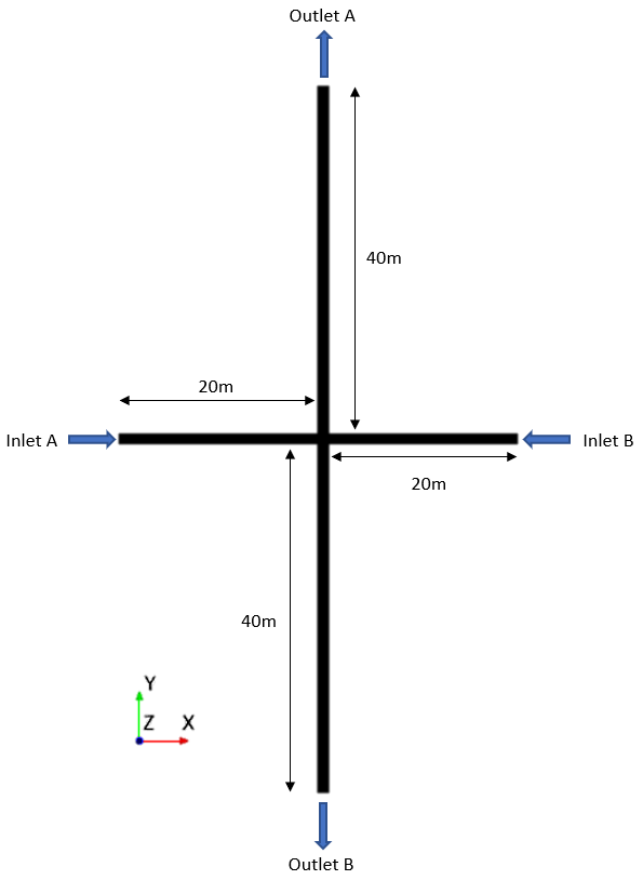

Figure 2- Top view of cross-slot configuration

The physics model chosen for the working fluid was a constant density, laminar, steady, three-dimensional flow. These conditions were chosen to emulate the best as possible the microfluidic conditions. The liquid that was chosen was water (H2O) with slightly different properties. The density was rounded from 997.6 kg/m^3 to 1000

kg/m^3 and the dynamic viscosity from 8.89x10^(-4) Pas to 1〖x10〗^(-3)Pas. This was done for the convenience of calculating the flow velocities for different generalised Reynolds values. The model of fluid that was chosen in the software was 'non-Newtonian Generalised Power Law' model.

This study performed ramp-down investigations on three separate power law index values (explained in the next section). These values were n=1 (Newtonian), n=0.8 (shear-thinning) and n=0.6 ("more" shear-thinning). The simulation investigations were initiated by imposing equal velocities in the inlet channels towards the intersection at high Generalised Reynolds value (above critical Reynolds value, Re=50 for Newtonian and Re=75 for non-newtonian). Once this was completed, the inertial flow instability at the meeting point was observed and measured. Two important numerical aspects of the simulations were analysed, the x-component of the velocity at the stagnation point using a line probe (line probe 2) to measure the data, at x=y=0, along the z-axis. The full profile was obtained and from that data the peak velocity was also recorded separately. Once the residuals stabilised and the results were constant and recorded, the imposed velocities at Inlet A and Inlet B were reduced by a value of 5 Reynolds number. Each time this was done, the data was recorded to observe the inertial flow instability and the axially-aligned vortex. When these phenomena were no longer present, it meant the generalised Reynolds number used for the flow was below the critical. To achieve more accurate results, the simulation model before the inertial instability disappeared is used again. This time decreasing the generalised Reynolds value by 1 each time to characterise when exactly does the inertial flow instability dissipate and the critical Reynolds value is passed. This process was done to view the intensities of the inertial flow instability under different conditions and to characterise the transition ramping-down from a steady-asymmetric flow to a steady-symmetric flow.

Four main derived parts were used to numerically record the results as well as visually represent rheological behaviours. The image seen in appendix 2 shows a scalar view of the cross-slot configuration used. It shows the important derived parts which are line probe 2, line probe 3, plane section and streamlines. The line probe 2 seen in the centre of the configuration was used to measure the inertial flow instability as mentioned previously. This probe was located at x=y=o, along the z-axis (0 - 1m). The characteristic stagnation point of this configuration is at the middle of this probe, as will be seen in the results section. Line probe 3 was placed along Inlet A to verify the development of the flow. It is located at z=0.5m, y=0 and spans along the x-axis (-20.5 - 0m). A different kind of derived part was also added, this was a plane section representing the x and z axis, normal to y-axis, as can be seen in Appendix 2. This visual aid of the flow firstly represents how the flow fully develops and how it interacts when reaching the intersection. The fourth important derived were streamlines which had the plane section as a source and continued into the outlet channels. These visually

represented the axially aligned spiral vortex which appears at high generalised Reynolds number.

4.0 Governing equations

This study performs a numerical investigation in which the inertial flow instability occurs in a cross-slot configuration. The power-law model (Poiseuille flow) is used to characterise Newtonian and shear-thinning fluids used in the simulations. The critical conditions in which the flow transitions from a steady-asymmetric flow to a steady-symmetric are investigated in a ramp-down process. The flow for the different working fluids investigated was considered as incompressible, laminar, steady and was evaluated using a three-dimensional volume mesh simulation using a finite-volume method.

The base equations solved using numerical methods are the equations of mass and momentum conservation as represented below:

$$\nabla * u = 0$$

Eq4

$$\rho\left(\frac{\delta u}{\delta t} + u * \nabla u\right) = -\nabla\rho + \nabla * \tau$$

Eq5

Where p is the pressure ρ is the density, u is the velocity vector and τ is the stress tensor (KON 6).

When studying conventional Newtonian fluids, the following Reynolds number is used as a dimensionless number to characterise the behaviour of the fluid. The Reynolds number is represented below:

$$Re = \frac{\rho U H}{\eta}$$

Eq6

U being the flow velocity, H is the height of the channel and η being the dynamic viscosity. This definition of the Reynolds number is good to use in cases where the viscosity remains constant. When investigating non-Newtonian fluids, other generalised Reynolds numbers must be used. As mentioned earlier, models are used to understand the most important characteristic features, therefore in this study a generalised Reynolds number will be used which removes the shear-thinning from the definition when using it with power law fluids. The generalised Reynolds number that will be used can be seen below:

$$Re_{gen} = \frac{6\rho U^{(2-n)} H^n}{K[\frac{4n+2}{n}]^n}$$

Eq7

Where n is the power law index, which defines the type of fluid to be modelled, k is the consistency index. K is equivalent with the dynamic viscosity when rearranging, making them have the same value. When using a power law index value of 1 (n=1), the original Newtonian expression for the Reynolds number is recovered [20]

In section 5, a validation process is performed comparing analytical results using equations and the results obtained from the Star CCM+ software. The initial validation is done in a 2D planar mesh using different power law index values, and using the velocity profile equation in Poiseuille flow through a slit, as seen below:

$$u_1 = \frac{2n+1}{n+1} U \left[1 - \left(\frac{x_2}{H} \right)^{\frac{n+1}{n}} \right]$$

Eq8

Where U is the imposed velocity at the start and the rest of the symbols maintain their meaning [14]. An easy way to visually verify if the results are on the right track is by calculating velocity as the centre (max. value) in a dimensionless manner diving it by U. When the power law index value is changed, the maximum velocity also changes, as will be seen in the validation section .

The 3D volume mesh straight channel is a bit more complex as the number of parameters increases. The equation used for the 3D validation can be seen below:

$$u(y,z) = \frac{16a^2}{\mu\pi^3}\left(-\frac{d\hat{p}}{dx}\right)\sum_{i=1,3,5\ldots}^{\infty}(-1)^{\frac{(i-1)}{2}}\left[1-\frac{\cosh\left(\frac{i\pi z}{2a}\right)}{\cosh\left(\frac{i\pi b}{2a}\right)}\right]x\frac{\cosh\left(\frac{i\pi y}{2a}\right)}{i^3}$$

Eq9

$$Q = \frac{4ba^3}{3\mu}\left(-\frac{d\hat{p}}{dx}\right)\left[1-\frac{192a}{\pi^5 b}\sum_{i=1,3,5\ldots}^{\infty}\frac{\tanh\left(\frac{i\pi b}{2a}\right)}{i^5}\right]$$

Eq10

Where $-a \leq y \leq a$ and $-b \leq z \leq b$, Q is the volumetric flow rate (m^3/s) [35]. The values of I in the summations was increased until the results variation was insignificant. The process to obtain the results was to first rearrange equation 10 in order to isolate $\left(-\frac{d\hat{p}}{dx}\right)$. Once all the iterations were complete, this was then included into equation 9, which then gave the analytical results for the velocity profile of a fluid flow along a rectangular section to validate.

5.0 Validation

In this section, the computational fluid dynamics software used (Star CCM+) is validated by creating some simple flow models and comparing them with analytical equations. This is done to make sure the results obtained from the simulation in section 6 are reliable. This is a two-step validation process. Firstly, a straight 2D planar mesh channel with constant dimensions is created to validate different power law indexes results with analytical equations. Any issues or mistakes ca be addressed at this stage to avoid difficulties when the model is more complex. Once this validation was completed successfully, a second validation was performed using a 3D volume mesh straight channel.

5.1 2D straight channel, power-law fluids velocity profiles

The graphs showing the results for this section will start with the Newtonian fluid and decreasing power law index value (n=1, n=0.6 and n=0.4. Section 6 will also follow this order to be able to compare the results for the non-Newtonian fluids (shear-thinning) with respect to the Newtonian (n=1). This validation used equation 7 for the generalised Reynolds number and equation 8 to obtain the analytical velocity profile. Table 1 shows the velocity values used for to achieve a generalised Reynolds value of 1, using three different power law index values. As mentioned previously, the consistency index has the same value as the dynamic viscosity. The consistency index, density and height are maintained constant while the imposed velocity at the inlet was varied to achieve a generalised Reynolds number of 1, to compare all the results. An extra column was added in table 1 to show the difference between both Reynolds definitions.

Table 1- Numerical parameters used to determine the generalised Reynolds number and the imposed velocity required for the 2D channel validation

n	Density	K (viscosity equivalent)	U	H	nominator	denominator	Re_{gen}	Re
1	1000	0.001	0.000001	1	0.006	0.006	1.000	1
0.6	1000	0.001	0.00003384	1	0.003306387	0.003305071	1.000	33.84
0.4	1000	0.001	0.00010051	1	0.002408164	0.002408225	1.000	100.51

For the first simulation, as stated, was the Newtonian fluid (n=1), which can be seen in figure 3. The results were obtained from the simulation using Star CCM+, where a line probe was placed with a resolution of 21 to match the resolution of the mesh. The results were extracted numerically from the software and placed in an excel sheet where it was compared with the set of results obtained from using equation 8. The horizontal axis shows the normalised y-position (where the line probe was placed), making a span of 1m. The vertical axis is the dimensionless normalised speed, where the speed was divided by the imposed speed (u/U). If equation 8 is solved using n=1, the maximum value matches the maximum value on the graph, being 1.5U. As it can also be seen in the figures, both the results and the analytical fit perfect upon each other making an expected smoothly curved velocity profile. This proved the 2D planar mesh for n=1 was validated successfully.

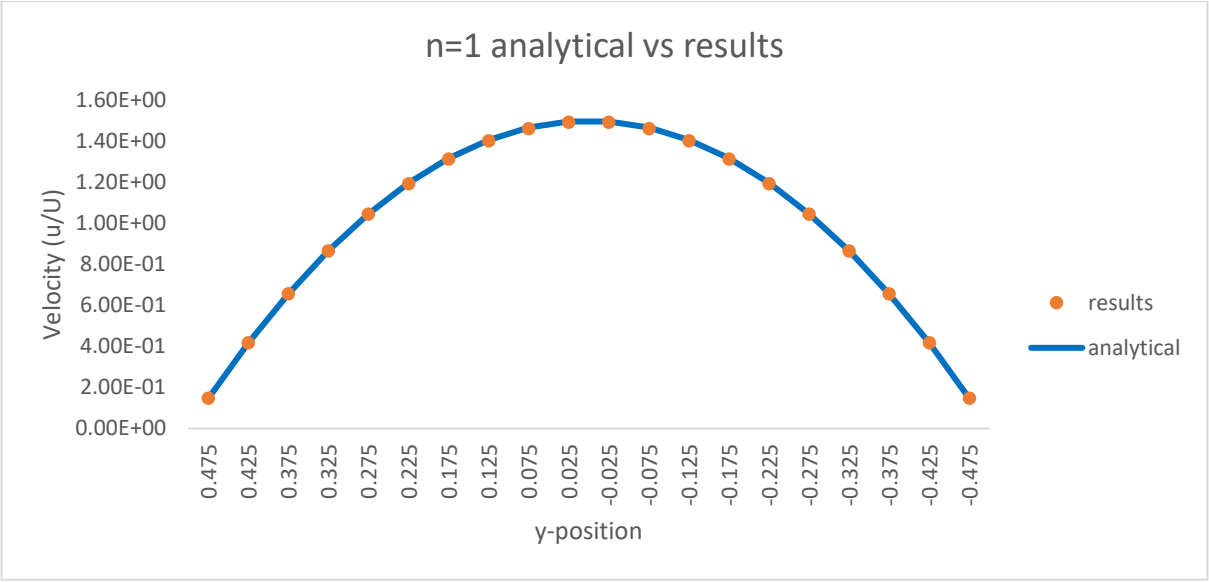

Figure 3- Numerical results of Star CCM+ vs analytical results of the velocity profile of fluid N=1 in a 2D channel

The second set of results in this section can be seen in figure 4. A power law index value of 0.6 was used in this model using the same procedure as with the Newtonian fluid previously. Figure 4 also shows how both the software results, and the analytical results overlap, making them match perfectly. When n=0.6 is included in equation 8 and solved, the maximum dimensionless value is 1.4U, once again matching with the results extracted from Star CCM+. This indicates that the methodology used to create the model in the software has been successful.

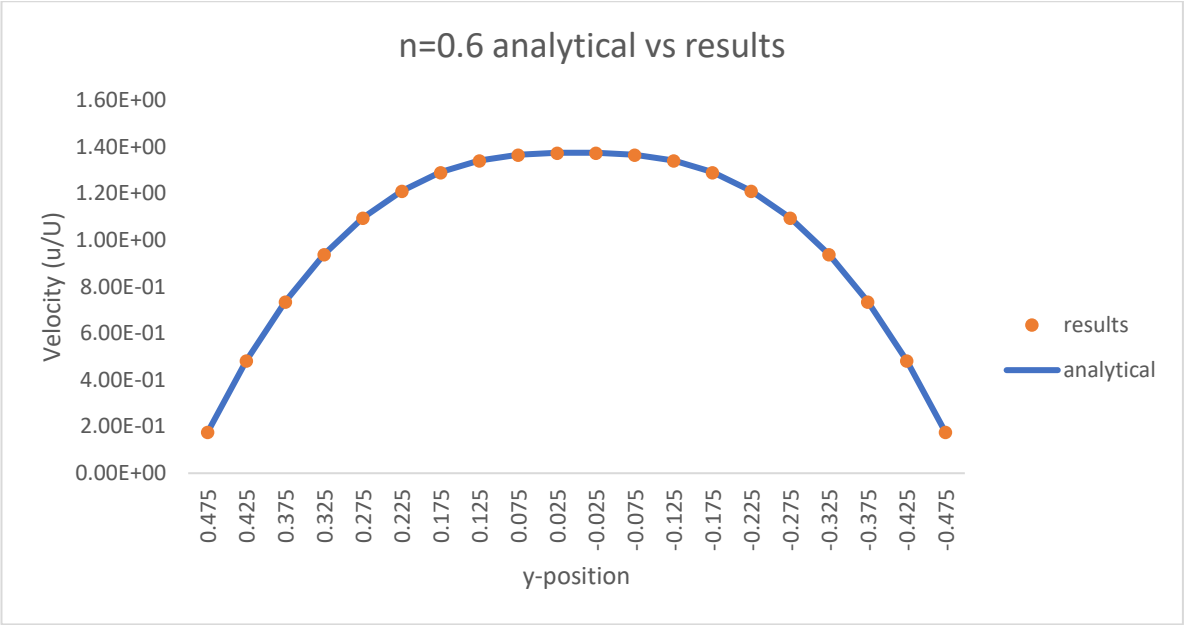

Figure 4- Numerical results of Star CCM+ vs analytical results of the velocity profile of fluid N=0.8 in a 2D channel

The last set of validation results in this section are in figure 5, which show the validation of a power law index value of 0.4 on the 2D straight channel. Same procedure was followed, proving equally successful. The analytical results match the software results perfectly, as the dimensionless maximum velocity is 1.3U for both.

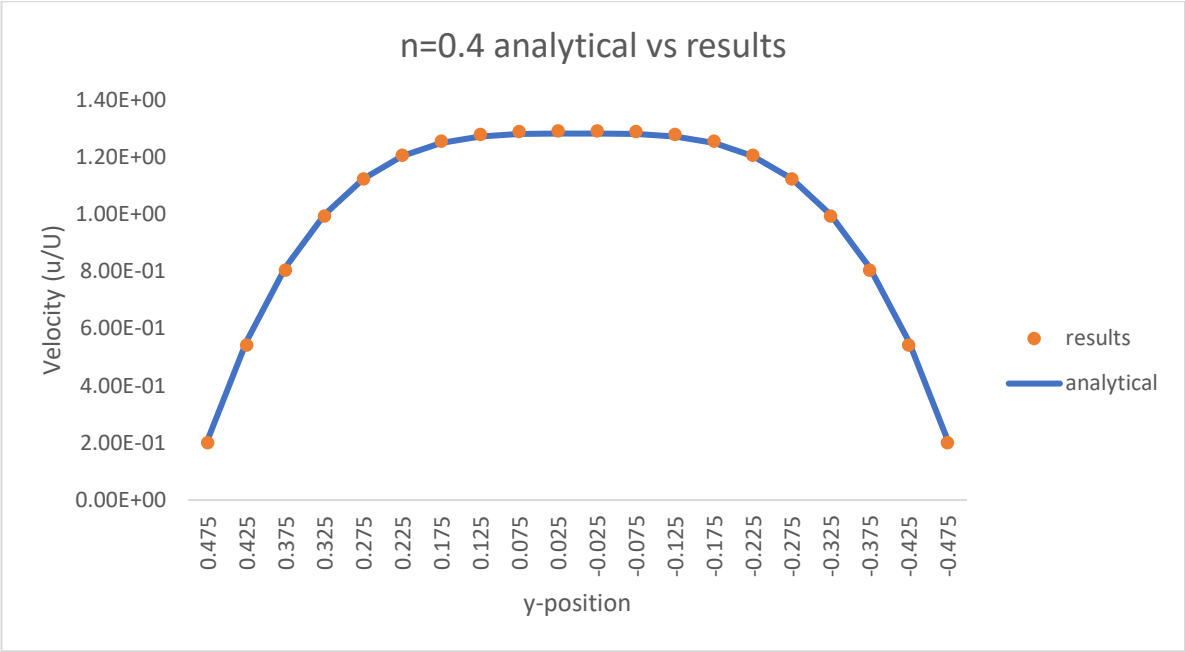

Figure 5- Numerical results of Star CCM+ vs analytical results of the velocity profile of fluid N=0.6 in a 2D channel

Figure 6 is a comparison between all 3 different power law index value velocity profile at a generalised Reynolds number of 1, as shown in table 1. It represents the difference in rheological behaviour this distinct property has. A way to describe this would be that n=1 has a lower gradient towards the walls but still achieves the highest peak amongst them. As the power law index value is decreased, the gradient of the line closer to the wall increases, but the centre region of the velocity profile flattens down the more shear-thinning the fluid is. The maximum velocities decrease from 1.5U, to 1.4U and finally 1.3U. This easily represents the impact of this property on the behaviour of the fluid.

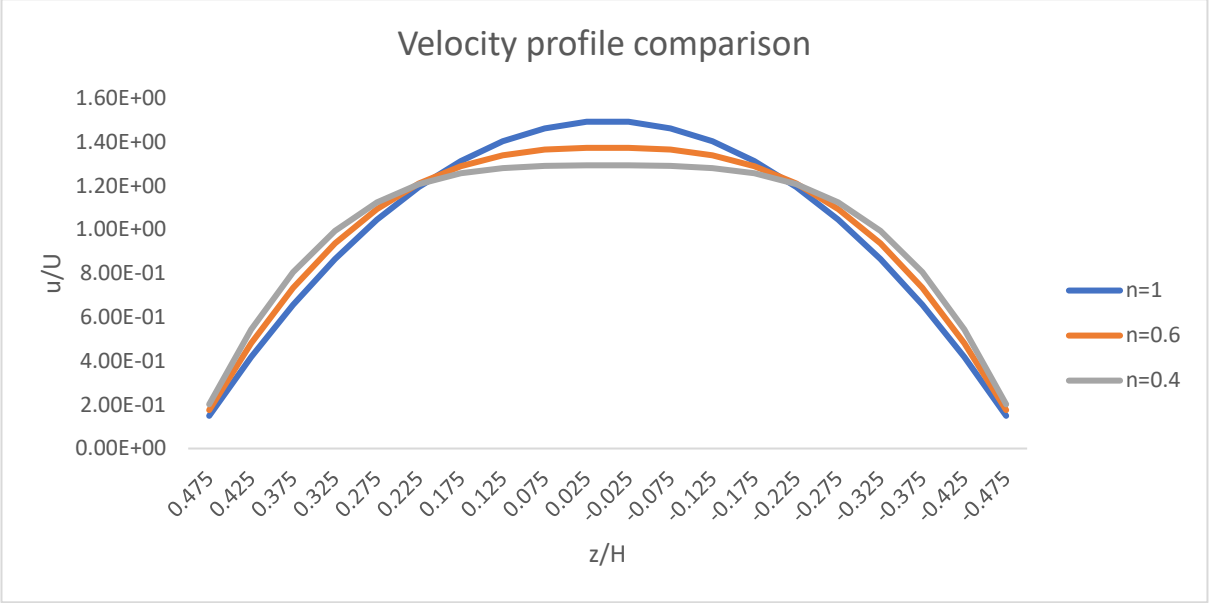

Figure 6- Comparison of the velocity profiles for the three different fluids in a 2D channel

5.2 3D straight channel, velocity profile

This sub-section proved to be significantly more challenging than the previous sub-section. This can be attributed to the added complexity of the 3D volume mesh straight square channel and the complex nature of equation 9 and equation 10 with respect to equation 8. Table 2 shows the imposed velocity used to achieve a generalise Reynolds number of 1, staying consistent with section 5.1 in order to model a square-section straight channel.

Table 2- Numerical parameters used to determine the generalised Reynolds number and the imposed velocity required for the 3D channel validation

n	density	K (viscosity equivalent)	U	H	nominmator	denominator	Re_{gen}	Re
1	1000	0.001	0.000001	1	0.006	0.006	1.000	1

Equation 9 and 10 were used to obtain analytical results for this section. The values used were a=0.5m, b=0.5m (square-section). The values of i were increased in both of the equations until the variation of the result of the summation was negligible. Equation 10 was rearranged in a manner to isolate $\left(-\frac{d\hat{p}}{dx}\right)$. This solution was then included into equation 9, performing all the iterations required to obtain a full analytical velocity profile.

When the analytical results were initially obtained using calculations in excel it matched perfectly with the results from the simulation, but due to a simple error in the excel analytical sheet, it had to be redone. The new analytical excel spreadsheet was obtained with accurate results but with a slight change. The new analytical results had 26 results in total. The initial results obtained from the simulated model were 20. This could be easily fixed but due to some issues with Star CCM+, the file could no longer be accessed. In appendix 3 a screenshot can be seen with the error encountered. The initial issue can be seen in appendix 4. The number of separate values differed between the correct analytical and the software results. This problem was initially addressed by modifying the resolution of the mesh (so that more velocities were calculated in the profile) and the resolution of the line probe used in Star CCM+. The technical problems occurring with the file adversely effected the results obtained. These effects can be seen in Appendix 5, where the simulation results gave the correct shape of the profile but with an unsmooth curve. The problem was not fixed by modifying the file model but by modifying the graph. As it can be seen in figure 7, the analytical results and the simulation results matched satisfyingly. The maximum values shown and the centre region behaviour show consistency.

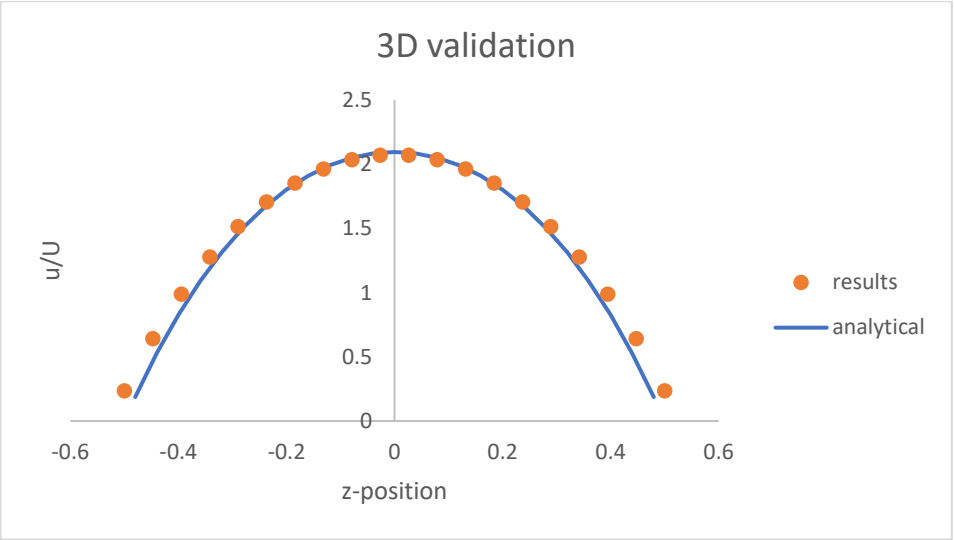

Figure 7- Numerical results of Star CCM+ vs analytical results of the velocity profile of fluid N=1 in a 3D channel

This validation is satisfactory, but as it can be spotted in figure 7 there is room for improvement. Both lines are not perfectly aligned close to the edge in the region beside the wall. This deviation could be improved by changing the mesh and line probe resolution so the same number is created in the model. By adding probes at the edge of the profile in the model, this would results in a more accurate results leading to a better validation.

6.0 Numerical results

This section contains the results of the investigation of the inertial flow instability on the 3D cross-slot simulation in Star CCM+ of the Newtonian and shear-thinning fluids, the validation using a mesh with a significantly higher resolution for each set of results as well as a verification that the flow along the inlet channels is fully developed before encountering the intersection. The strategy to illustrate the results for the inertial flow instability for the different fluids was to initially obtain the results from the Newtonian, then the results for both shear-thinning fluids are compared with the equivalent Newtonian behaviour as a reference. This will be presented in section 6.1.. In this study, ramps are done only down in generalised Reynolds number to investigate the transition from steady-asymmetric to steady-symmetric flow, obtaining the critical generalised Reynolds number which characterises the offset of the instability. The results for the different ramp-down velocity profiles of the x-axis velocity magnitude located at the stagnation point in x=y=0 along the z-axis are presented in presented obtaining the numerical results using line probe 2, that can be seen in appendix 2. The maximum values for each different generalised Reynolds number are then extracted and presented in a different graph so that the characteristics of the rheological behaviour can be studied. An additional table is included which contains the value of the main generalised Reynolds numbers which characteristics the behaviour, such as the critical generalised Reynolds number. When some results are presented using a computational fluid dynamics software, a process of validation much be done. Section 6.2. contains the validation process performed for each different fluid. This was completed by comparing the original results with the equivalent results of a mesh with a higher resolution, making sure that the variation when compared was acceptable and spot any difference in behaviour. This simulation was extensively more computationally demanding and required almost 12 hours for the residuals to stabilise. This allows the results presented in this investigation to be more reliable. To finish the numerical results section, a verification of the fully developed inlet velocity profile of the flow is included. The flow is initially imposed with equal velocity throughout the cross-section at the start of both inlet channels. Section 6.3. shows the results extracted from line probe 3 shown in appendix 3 for the different fluids investigated at the same generalised Reynolds number. This makes sure the

velocity profile is fully developed and behaves appropriately when encountering the intersection.

6.1 Results and discussion

In this section the core of the numerical results obtained in this investigation are presented. Three different fluids were modelled, these were a Newtonian fluid (n=1) and two Shear-thinning (n=0.8 and n=0.6). The Newtonian results which exhibit its response to the characteristics of this particular model are presented first to have a reference of comparison.

The simulations were initiated at high Reynolds number (above critical generalised Reynolds number) performing ramp down in generalised Reynolds number. For this reason, all of the evaluations begin from an initial steady-asymmetric solution, and as the generalised Reynolds number is reduced until it transitions to a steady-symmetric solution. The intervals between the gen Reynolds number above or below the transition region are of 5, significantly higher than in the area of interest. The region of generalised Reynolds number where the transition occurs in investigated in higher precision varying the values of the generalised Reynolds value in steps of 1 as will be seen in the graphs. These results will show the difference in rheological behaviour between a Newtonian fluid and two shear-thinning fluids with different power law index in a cross-slot configuration. The results were presented in a dimensionless manner so that the key characteristic behaviours obtained from the results can be extrapolated to other investigations.

6.1.1 N=1

As discussed earlier, the results for the Newtonian fluid will be presented first. The amount of existing literature involving Newtonian flows is extensive, so certain

behaviours can be anticipated. Table 3 shows a list of the different generalised Reynolds number used in the ramp down in this model. As discussed, the generalised critical Reynolds number is well known for a Newtonian fluid, so a generalised Reynolds number of 50 was chosen to initiate the ramp down. As seen in the table, all the dimensions and properties of the model are maintained constant through the ramp down, only changing the imposed velocity at the inlet of the inlet channels to alter the generalised Reynolds number. It can be seen in column 9 in table 3 that when using a Newtonian fluid, the original Reynolds definition is recovered, showing no difference between both. Thanks to the approximations done with the fluid properties, the velocities imposed are much "nicer" than if this wouldn't have been done.

Table 3- Numerical parameters used to determine the generalised Reynolds number and the imposed velocity required for the cross-slot geometry model with fluid N=1

n	denstiy	K (viscosity equivalent)	U	H	nominmator	denominator	Re_{gen}	Re
1	1000	0.001	0.00005	1	0.3	0.006	50.000	50
1	1000	0.001	0.000045	1	0.27	0.006	45.000	45
1	1000	0.001	0.0000425	1	0.255	0.006	42.500	42.5
1	1000	0.001	0.000041	1	0.246	0.006	41.000	41
1	1000	0.001	0.00004	1	0.24	0.006	40.000	40
1	1000	0.001	0.000039	1	0.234	0.006	39.000	39
1	1000	0.001	0.000037	1	0.222	0.006	37.000	37
1	1000	0.001	0.000035	1	0.21	0.006	35.000	35
1	1000	0.001	0.00003	1	0.18	0.006	30.000	30

The inertial instability is shown in figure 8 for the Newtonian fluid, the numerical results extracted from line probe 2 were used to construct this graph. It clearly exhibits the inertial flow instability at high gen Reynolds number, decreasing in

strength as the value is decreased. A key characteristic behaviour of the cross-slot configuration can be spotted in the graph. This is the stagnation point located at the centre, having a velocity magnitude of zero as expected for all of the different simulations. The maximum velocity of the central vortex on both sides tends to be placed in the same location through the ramp down, which would be about 70% of the way from the boundary to the centre (stagnation point). The maximum dimensionless velocity at a generalised Reynolds value of 50 is u/U=2.02, which decreases during the ramp down, exhibiting the reduction in strength of the instability indicating the nearing of the transition. The results for a generalised Reynolds number of 40 are the last time the inertial flow instability can be observed. Next value that was simulated was a generalised Reynolds value of 39, where the flow had already transitioned from steady-asymmetric to steady-symmetric. The flow inertial instability is no longer present. All the results after the critical Reynolds number should be zero, the difference in the graph is due to numerical error in the model. This could be improved by increasing the resolution of the volume mesh.

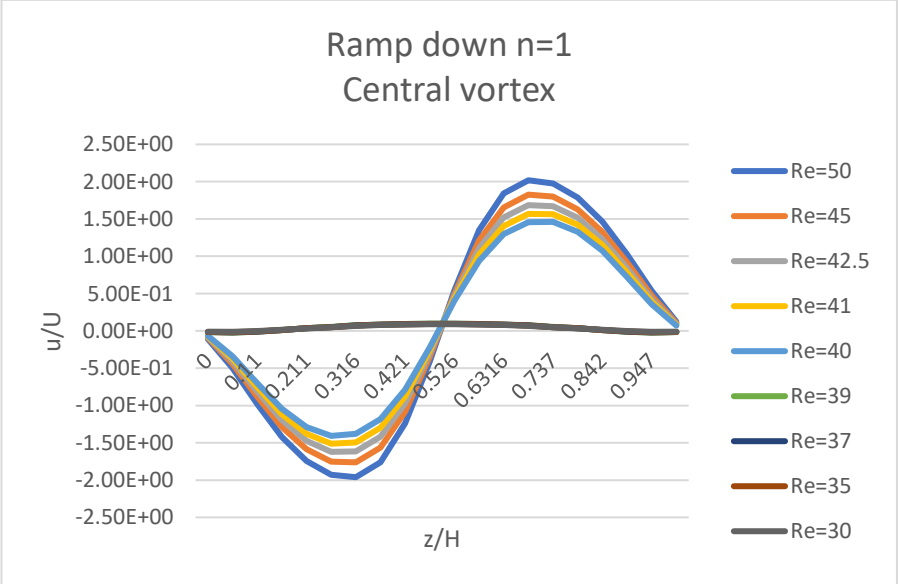

Figure 8- Numerical results from Star CCM+ of the x-component velocity obtained from line probe 2 for fluid N=1 ramp down in generalised Reynolds number

Figure 9 is a Ramp down map of the maximum velocities from each of the different simulations. The value at a generalised Reynolds of 50 is consistent with figure 8. This graph has the dimensionless velocity as the vertical axis, the horizontal axis is the generalised Reynolds number imposed. The horizontal steps vary, above and

below the transition region the steps have a variation of 5, while in the transition region the steps variation is reduced to 1. This enables a closer look at the transition, being able to pinpoint closer the generalised Reynolds number that offsets the inertial instability. It shows the steady-asymmetric flow with the inertial instability behaviour decreasing gradually up to a generalised Reynolds of 40, where at 39 it is not present anymore, meaning the critical generalised Reynolds number lies between 39 and 40. The numerical error mentioned before can also be spotted in figure 9, as all of the results for generalised Reynolds of 39 and lower are not perfectly aligned with zero.

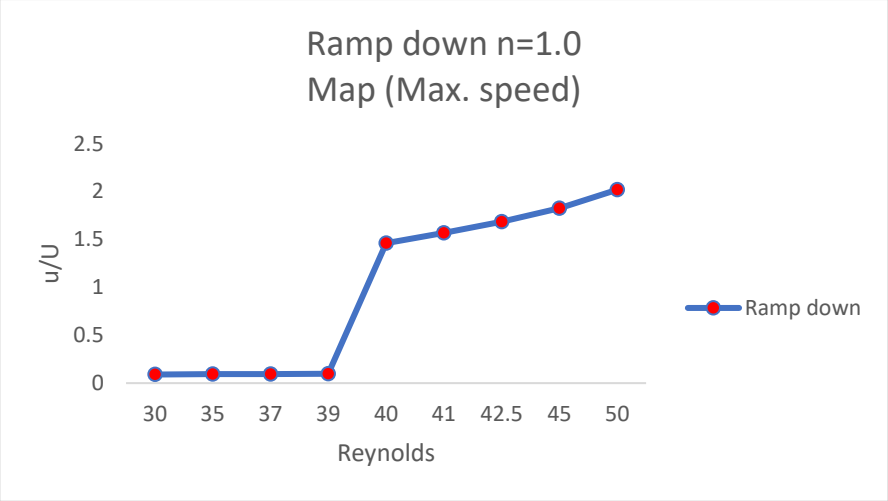

Figure 9- Ramp down map depicting the maximum velocity of the central vortex for each different generalised Reynolds number for fluid N=1

The final processed results for the Newtonian fluid can be seen in table 4. The different behaviours and the presence of the inertial instability is classified depending on the imposed velocities.

Table 4- Characterisation of the behaviour of the flow depending on the generalised Reynolds number imposed for fluid N=1

regen	**Flow behaviour**	**Inertial instability**
$40 \leq$ regen	Steady-asymmetric	present
$39 <$ regen < 40	transition	dissipating
Regen ≤ 39	Steady-symmetric	Not present

6.1.2 N=0.8

The results for the shear-thinning (n=0.8) fluid will be presented here. As mentioned in section 2, there is less existing literature about non-Newtonian fluids than for the Newtonian case. Also, within the literature for non-Newtonian fluids, the focus of investigations is more focused in Low Reynolds number. For this reason, the initial imposed generalised Reynolds number for both shear-thinning fluids (n=0.8 and n=0.6) is 75. Table 5 contains the properties and dimensions used to complete the simulation of the n=0.8 mode. When a power law index is introduced which is not n=1 (Newtonian) there is a curious effect, the difference between the two Reynolds number differs massively with respect to table 3. The original definition for Reynolds number is not recovered, as seen in column 9 in the table.

Table 5- Numerical parameters used to determine the generalised Reynolds number and the imposed velocity required for the cross-slot geometry model with fluid N=0.8

n	denstiy	K (viscosity equivalent)	U	H	nominmator	denominator	Re_{gen}	Re
0.8	1000	0.001	0.00028578	1	0.33526595	0.004470238	75.000	285.78
0.8	1000	0.001	0.00026981	1	0.312911051	0.004470238	69.999	269.81
0.8	1000	0.001	0.00025366	1	0.290571915	0.004470238	65.001	253.66
0.8	1000	0.001	0.00023729	1	0.268217169	0.004470238	60.001	237.29
0.8	1000	0.001	0.00022069	1	0.245861449	0.004470238	55.000	220.69
0.8	1000	0.001	0.00020384	1	0.223510816	0.004470238	50.000	203.84
0.8	1000	0.001	0.00018671	1	0.201164965	0.004470238	45.001	186.71
0.8	1000	0.001	0.00016925	1	0.178807472	0.004470238	40.000	169.25
0.8	1000	0.001	0.00016572	1	0.174341653	0.004470238	39.001	165.72
0.8	1000	0.001	0.00016217	1	0.169869681	0.004470238	38.000	162.17
0.8	1000	0.001	0.00015861	1	0.165404731	0.004470238	37.001	158.61
0.8	1000	0.001	0.00015502	1	0.160922411	0.004470238	35.999	155.02
0.8	1000	0.001	0.00015143	1	0.156460804	0.004470238	35.001	151.43
0.8	1000	0.001	0.00013317	1	0.134103135	0.004470238	29.999	133.17
0.8	1000	0.001	0.0001144	1	0.111753846	0.004470238	25.000	114.4

The results for the ramp down in generalised Reynolds number for the n=0.8 fluid can be seen in figure 10. The first noticeable thing that can be spotted in the resemblance in shape to the Newtonian fluid simulation in figure 8, not exhibiting any obvious difference in behaviour. The stagnation point at the centre is also present. The graph shows that as the ramp down is taking place, the strength of the inertial instability reduces. If compared with the Newtonian case, the maximum velocity is also placed about 70% of the way from the boundaries to the centre. This means that the inertial instability rheological characteristics haven't changed in that matter. To further compare with the Newtonian case, the maximum velocity values suffer a slight variation, may be numerical error. The maximum velocity at generalised Reynolds number of 50 for the n=0.8 fluid is u/U=2.09, being a slight increase of 3.5%.

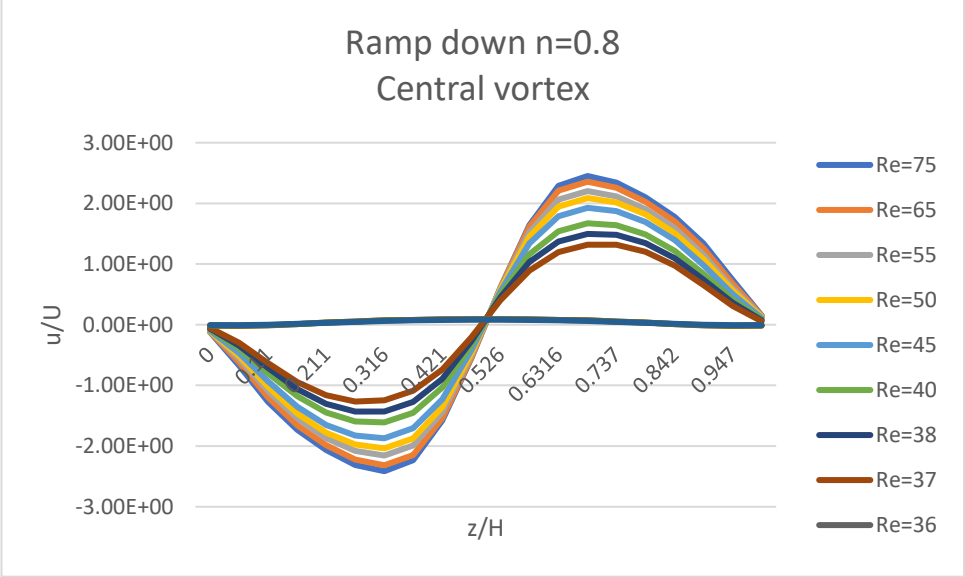

Figure 10- Numerical results from Star CCM+ of the x-component velocity obtained from line probe 2 for fluid N=0.8 ramp down in generalised Reynolds number

The most noticeable difference between both cases can be seen in the transition from steady-asymmetric to steady-symmetric. As it can be seen in both figure 11 and figure 10, the inertial flow instability dissipates between 37 to 36. This is noticeably lower than the Newtonian case. Another peculiar characteristic is that at a generalised Reynolds number of37, the inertial flow instability still exists with a much smaller strength (u/U=1.32) than when the Newtonian fluid transitioned. This

means that this fluid model could maintain the inertial instability longer in a ramp-down process.

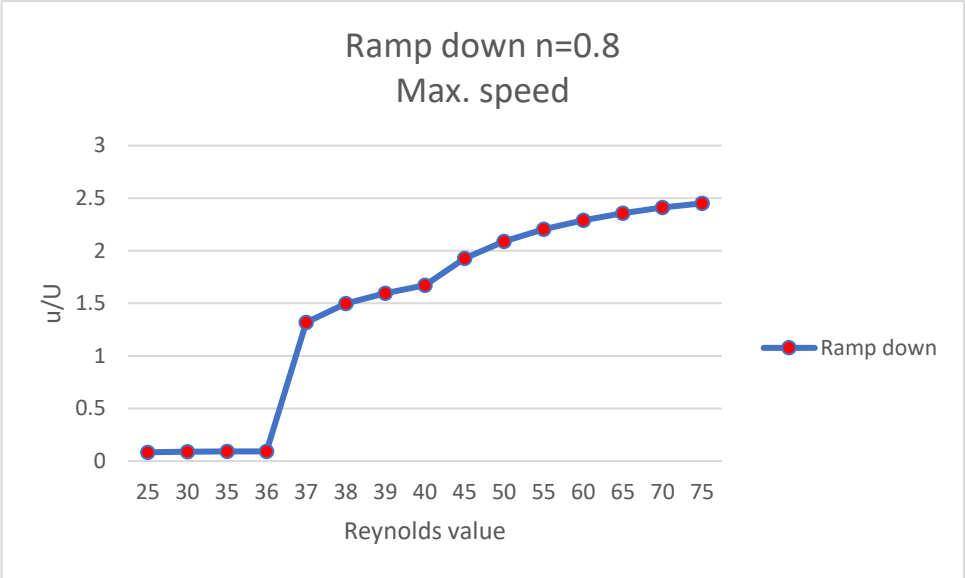

Figure 11- Ramp down map depicting the maximum velocity of the central vortex for each different generalised Reynolds number for fluid N=0.8

The processed results for the n=0.8 shear-thinning fluid are presented in table 6. Here it shows that the transition from steady-asymmetric to steady-symmetric occurs between 37 and 36.

Table 6- Characterisation of the behaviour of the flow depending on the generalised Reynolds number imposed for fluid N=0.8

regen	Flow behaviour	Inertial instability
$37 \leq$ genre	Steady-asymmetric	Present
$36 <$ genre < 37	Transition	Dissipating
genre ≤ 36	Steady-symmetric	Not present

6.1.3 N=0.6

The fluid used in the simulation for this section has the lowest value of power law index. This means that it has the most shear-thinning behaviour out of the three fluids investigated in this study. The numerical results for the n=0.6 fluid presented in this section were obtained in the same way as the previous fluids. As with the n=0.8 fluid, the ramp down in generalised Reynolds number was initiated at a value of 75. Table 7 shows the different imposed velocities that were used, while maintaining all the properties and dimensions constant. Column 9 shows the immense difference between the two Reynolds number values, showing that the further away the power law index goes from 1, the bigger the difference will be between both definitions.

Table 7- Numerical parameters used to determine the generalised Reynolds number and the imposed velocity required for the cross-slot geometry model with fluid N=0.6

n	denstiy	K (viscosity equivalent)	U	H	nominmator	denominator	Re_gen	Re
0.6	1000	0.001	0.00073899	1	0.24788214	0.003305071	75.001	738.99
0.6	1000	0.001	0.00066718	1	0.214828293	0.003305071	65.000	667.18
0.6	1000	0.001	0.00059214	1	0.181779711	0.003305071	55.000	592.14
0.6	1000	0.001	0.00055317	1	0.165254509	0.003305071	50.000	553.17
0.6	1000	0.001	0.00051307	1	0.14872998	0.003305071	45.001	513.07
0.6	1000	0.001	0.00047167	1	0.132204064	0.003305071	40.000	471.67
0.6	1000	0.001	0.00046321	1	0.128896269	0.003305071	39.000	463.21
0.6	1000	0.001	0.0004547	1	0.125593217	0.003305071	38.000	454.7
0.6	1000	0.001	0.00044612	1	0.122287938	0.003305071	37.000	446.12
0.6	1000	0.001	0.00043747	1	0.118981335	0.003305071	36.000	437.47
0.6	1000	0.001	0.00042876	1	0.115678119	0.003305071	35.000	428.76
0.6	1000	0.001	0.00038406	1	0.099153936	0.003305071	30.001	384.06
0.6	1000	0.001	0.00033716	1	0.082626948	0.003305071	25.000	337.16

Numerical results obtained from the line probe 2 for the n=0.6 are presented below, in figure 12. As the graph shows, the shape of the velocity profiles is identical to those for the Newtonian fluid and other shear-thinning (n=0.8). The maximum velocity of each simulation was at the same location, this being about 70% of the way from the boundary to the centre of the intersection, where the stagnation point is located. The maximum velocity at genre=50 was a dimensionless velocity u/u=2.07, showing once again a slight increase with respect to the Newtonian fluid, barely below the equivalent maximum velocity for the n=0.8 shear-thinning fluid.

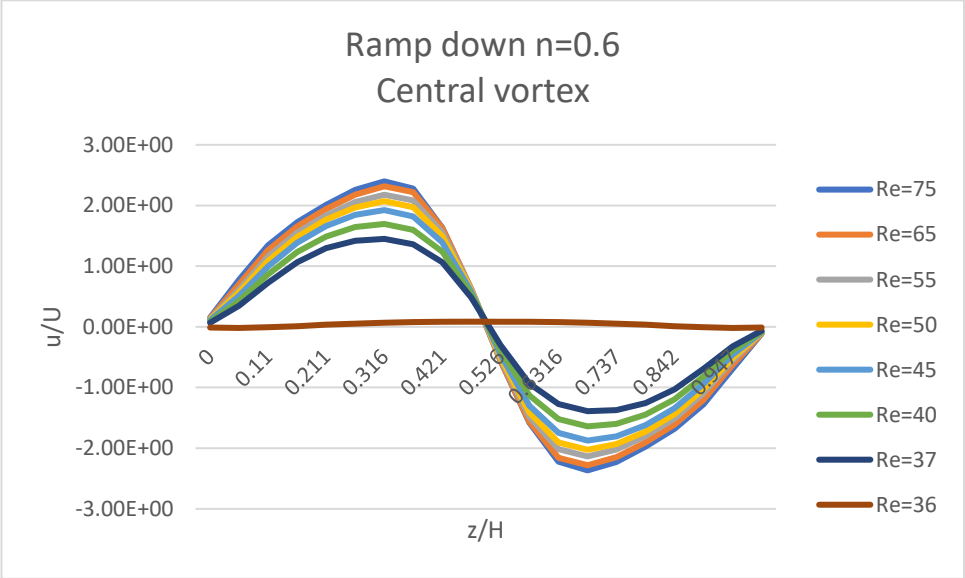

Figure 12- Numerical results from Star CCM+ of the x-component velocity obtained from line probe 2 for fluid N=0.8 ramp down in generalised Reynolds number

The strength of the inertial vorticity can be observed to decrease as the ramp down in generalised Reynolds number. The interesting detail is that the transition occurs in between the same generalised Reynolds values as with the other shear-thinning fluid (n=0.8), transitioning from steady-asymmetric to steady-symmetric between genre 37 and 36. This can also be seen in the ramp down map in figure13, exhibiting a identical behaviour to the n=0.8 fluid. The dimensionless maximum velocity at a generalised Reynolds of 37 at the last point present was u/U=1.45.

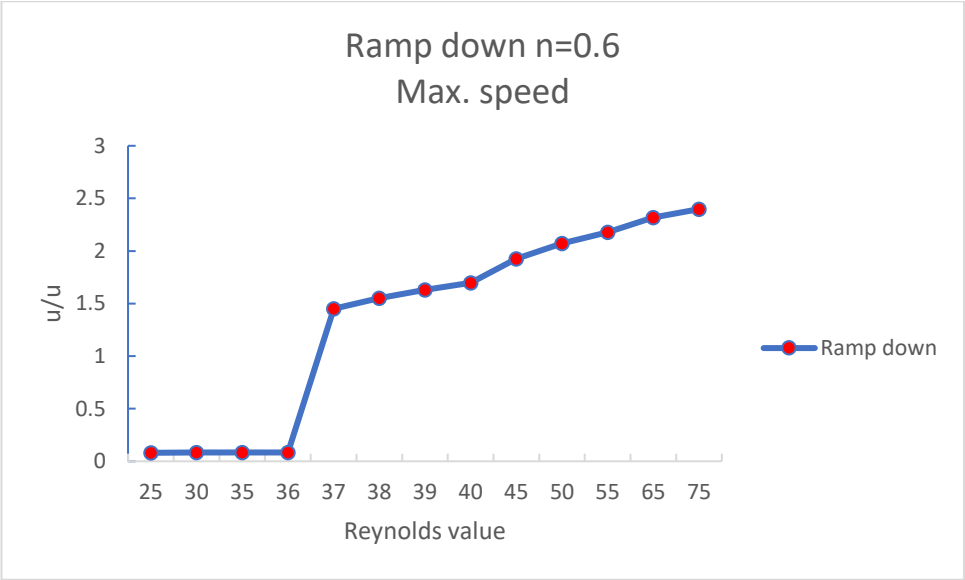

Figure 13- Ramp down map depicting the maximum velocity of the central vortex for each different generalised Reynolds number for fluid N=0.6

The processed results for the n=0.6 fluid modelled is shown in table 8 where the critical generalised Reynolds value is presented as well as the behaviour to be expected at different imposed generalised Reynolds number. The transition happens at the same equivalent value and in an identical manner. Appendix 6 shows a graph where the central vortex of the three different fluids is presented with equivalent generalised Reynolds. The graphs are almost identical, having a slight increase at the peak of the vortices in each side.

Table 8- Characterisation of the behaviour of the flow depending on the generalised Reynolds number imposed for fluid N=0.6

genre	**Flow behaviour**	**Inertial instability**
$37 \leq$ genre	Steady-asymmetric	present
$36 <$ genre < 37	Transition	Dissipates
Genre ≤ 36	Steady-symmetric	Not present

6.2 Validation

Once the initial validations, like those in section 5, have been done and the results have been recorded, it is common practice to perform further validation. When a computational fluid dynamics model is used for investigation, a popular technique for further validation is to construct a significantly more refined and complex model and run the model under the same conditions so that the results can be checked. The results are analysed to make sure the variation is within an acceptable range. The reason the models used for the results are simpler than the validation model is due to its computational demand and high-capacity requirement. Increasing the mesh is the slightest increases the computations needed for stabilised results. The different body meshes are interconnected between them, meaning that if a property wants to be modified, by doing it in on the source meshes, the whole configuration will be updated. The original model base size of the mesh was 0.05m, this was reduced to 0.01m. The values for the one-sided geometric sequence in the inlet channels was maintained, due to its smooth refinement with the intersection body. The outlet channels on the other hand were additionally modified. The number of layers of the one-sided geometric sequence was increased from 45 layers to 63 layers to match the refinement of the mesh at the intersection. This can be seen in appendix 7, where a top view of the intersection is showed to observe the difference in the more refined model. The following graphs show the results for this additional process of validation. Figure 14 contains the validation for the Newtonian fluid. It can be observed that the general shape is maintained, with a slight increase in the maximum velocity from u/U=2.02 to u/U=2.07.

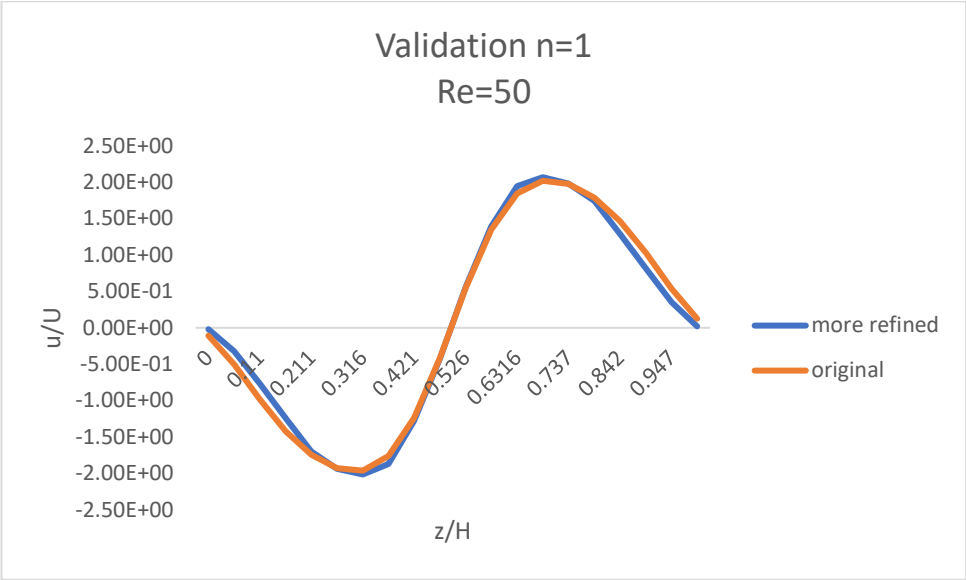

Figure 14- Validation by comparing original mesh results with a more refined mesh results at Generalised Reynolds number of 50 for fluid N=1

Figure 15 and 16 show the validation process for both shear-thinning fluid (n=0.8 and n=0.6). It follows the same variation behaviour as for the Newtonian fluid validation. The three validation results show two common differences between the original model and the more refined. The maximum speeds of the inertial instability at both sides increases in the slightest. The second common difference is the region close to the walls. Both results don't match as accurately as elsewhere. The gradient for the more refined model increases more progressively when starting from the walls, staying right under the original model results in that region. Overall, this validation is successful as no significant differences were noted that could affect the results in section 6.1.

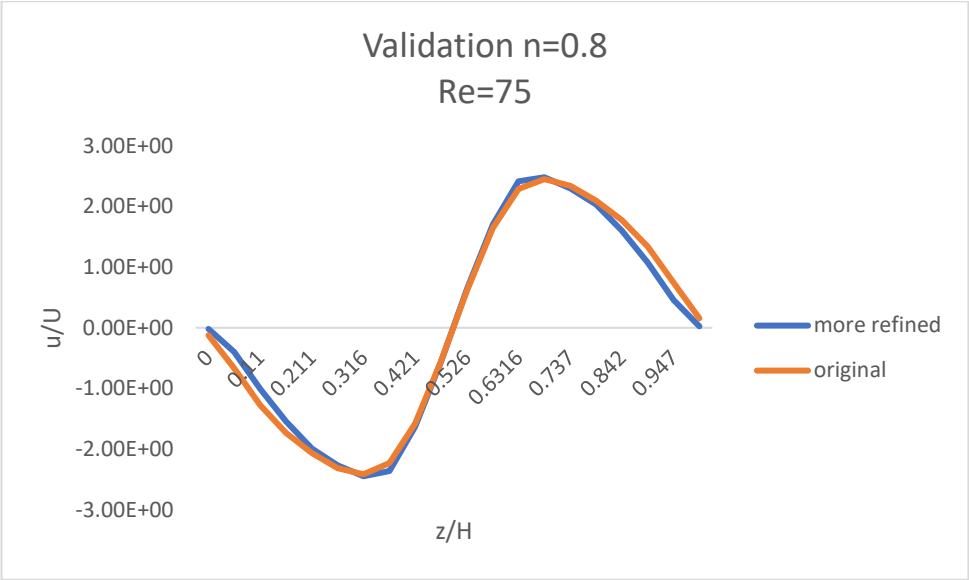

Figure 15- Validation by comparing original mesh results with a more refined mesh results at Generalised Reynolds number of 75 for fluid N=0.8

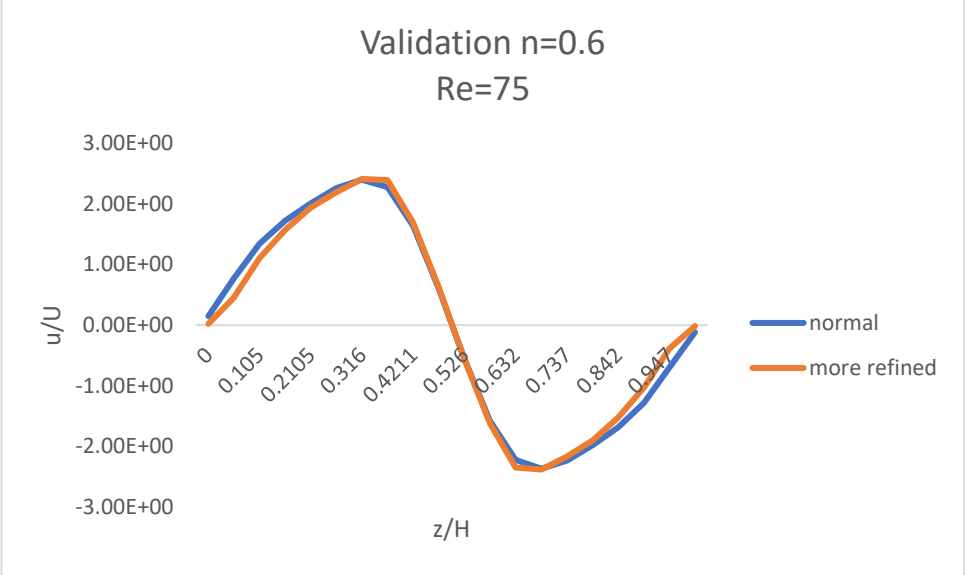

Figure 16- Validation by comparing original mesh results with a more refined mesh results at Generalised Reynolds number of 75 for fluid N=0.6

6.3 Development velocity profile

This section contains the last set of numerical results of this investigation. When using complex geometric configurations (especially multi-stream) many different things have to be considered and verified with respect to the particular characteristics and rheological properties. In addition, simple characteristics also have to be verified. Both inlet channels in the cross-slot configuration were designed with lengths of 20m along the x-axis in order to allow the imposed flow to transition to a fully developed velocity profile before reaching the intersection. Line probe 3, as seen in appendix 2 was used to obtain these results. This probe was placed at the centre of the inlet channels (y=0 and z=0.5) and along the x-axis to record the development of the inlet flow. Figure 17 shows the results for the three different fluids investigated at equivalent generalised Reynolds number of 50. The shape of the results show an expected similarity in behaviour, started at a certain value and increasing to the fully developed velocity profile velocity until it finally encounters the stagnation point at the centre of the configuration, where the velocity decreases until zero within the intersection body. Another expected characteristic is that as the power law index decreases, so does the dimensionless velocity. These results verify the inlet channels were fully developed and that the inertial instability investigated was not affected by undeveloped flows.

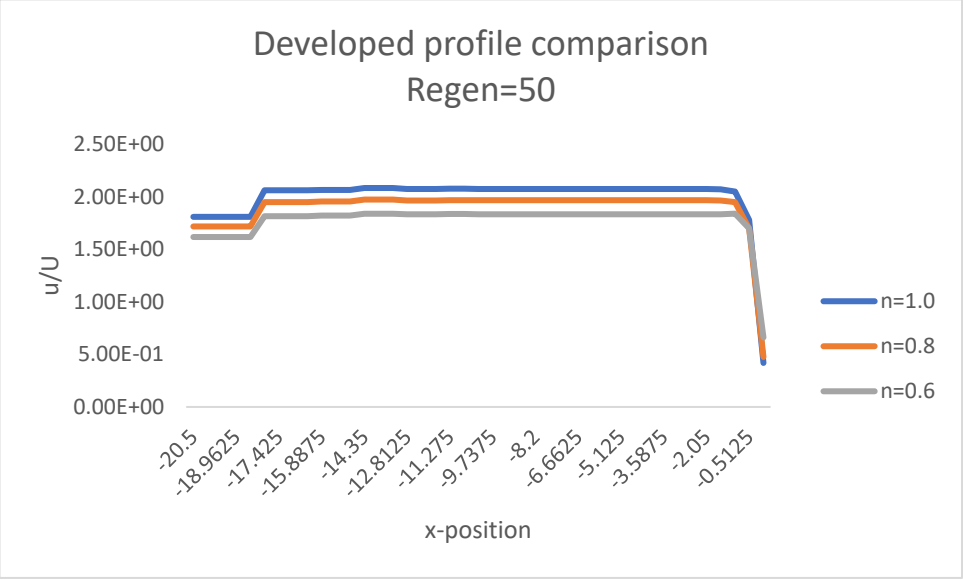

Figure 17- Numerical results obtained from line probe 3 for the verification of the fully developed flow

7.0 Conclusion

A numerical study was done on the effects of shear-thinning fluids in a three-dimensional cross-slot configuration of aspect ratio of 1. Three different fluids were simulated following the power law model and a generalised Reynolds number expression was utilised. An initial validation was undertaken to give a level of confidence to the results. A ramp down in generalised Reynolds number permitted the characterisation of the behaviour of the flow, starting as a steady-asymmetric flow with the presence of an inertial instability, the transition during the ramp down, and the steady-symmetric flow.

The results presented in section 6 demonstrate some different behaviours. It was seen that both shear-thinning fluids maintained the shape of the inertial instability but required a lower generalised Reynolds number to provoke the transition. This means that the axially aligned spiral vortex and the steady-asymmetric flow was observed at a generalised Reynolds value where the equivalent Newtonian fluid has already transitioned to a steady-symmetric. Another phenomenon that could be observed when comparing results is that the figures for the central vortex for the Newtonian fluid and n=0.8 fluid started negative, while the n=0.6 fluid started positive, meaning the inertial instability has no fixed preference on direction.

The reduction in the critical generalised Reynolds number could be useful for many applications. One of the many applications discussed in section 2 mentioned using the inertial instability that occurs in the intersection for the purpose of mixing in microfluidic streams. An energy input is required to impose a flow in real life systems, therefore by using a fluid with shear-thinning with a lower generalised Reynolds number imposed it could reduce energy required on the wanted imposed flow while maintaining the mixing properties due to the presence of the inertial instability.

8.0 References

[1] Tanner, R.I., 2000. *Engineering rheology* (Vol. 52). OUP Oxford.

[2] Malkin, A.Y. and Isayev, A.I., 2017. *Rheology: concepts, methods, and applications*. Elsevier.

[3] Barnes, H.A., Hutton, J.F. and Walters, K., 1989. *An introduction to rheology* (Vol. 3). Elsevier.

[4] Spencer, A.J.M., 2004. *Continuum mechanics*. Courier Corporation.

[5] Temam, R., 2001. *Navier-Stokes equations: theory and numerical analysis* (Vol. 343). American Mathematical Soc..

[6] https://blog.rheosense.com/non-newtonian-fluid-modeling-power-law-model

[7] Tabeling, P., 2005. *Introduction to microfluidics*. OUP Oxford.

[8] Bassous, E., Taub, H.H. and Kuhn, L., 1977. Ink jet printing nozzle arrays etched in silicon. *Applied Physics Letters*, *31*(2), pp.135-137.

[9] Terry, S.C., Jerman, J.H. and Angell, J.B., 1979. A gas chromatographic air analyzer fabricated on a silicon wafer. *IEEE transactions on electron devices*, *26*(12), pp.1880-1886.

[10] Gravesen, P., Branebjerg, J. and Jensen, O.S., 1993. Microfluidics-a review. *Journal of micromechanics and microengineering*, *3*(4), p.168.

[11] Froese, R., 2006. Cube law, condition factor and weight–length relationships: history, meta-analysis and recommendations. *Journal of applied ichthyology*, *22*(4), pp.241-253.

[12] Sahin, M. and Owens, R.G., 2004. A numerical investigation of wall effects up to high blockage ratios on two-dimensional flow past a confined circular cylinder. *Physics of fluids*, *16*(5), pp.1305-1320.

[13] Goldburg, A. and Florsheim, B.H., 1966. Transition and Strouhal number for the incompressible wake of various bodies. *The Physics of Fluids*, *9*(1), pp.45-50.

[14] Bharti, R.P., Chhabra, R.P. and Eswaran, V., 2007. Two-dimensional steady Poiseuille flow of power-law fluids across a circular cylinder in a plane confined channel: wall effects and drag coefficients. *Industrial & engineering chemistry research*, *46*(11), pp.3820-3840.

[15] Chen, L.S., Polifke, W., Hosseini, N., Teerling, O.J., Arteaga, I.L., Kornilov, V. and de Goey, P., 2016. Acoustic scattering behavior of a 2D flame with heat exchanger in cross-flow. In *Proceedings of the 23rd International Congress on Sound and Vibration*.

[16] Ruz, O., Castillo, E., Cruchaga, M. and Aguirre, A., 2021. Numerical study of the effect of blockage ratio on the flow past one and two cylinders in tandem for different power-law fluids. *Applied Mathematical Modelling*, *89*, pp.1640-1662.

[17] Gao, B., Bi, Q., Nie, Z. and Wu, J., 2015. Experimental study of effects of baffle helix angle on shell-side performance of shell-and-tube heat exchangers with discontinuous helical baffles. *Experimental thermal and fluid Science*, *68*, pp.48-57.

[18] Schultze, L.K.P., Merckelbach, L.M., Horstmann, J., Raasch, S. and Carpenter, J.R., 2020. Increased mixing and turbulence in the wake of offshore wind farm foundations. *Journal of Geophysical Research: Oceans*, *125*(8), p.e2019JC015858.

[19] Robertson, A.M., Sequeira, A. and Owens, R.G., 2009. Rheological models for blood. In *Cardiovascular mathematics* (pp. 211-241). Springer, Milano.

[20] Dhinakaran, S., Oliveira, M.S.N., Pinho, F.T. and Alves, M.A., 2013. Steady flow of power-law fluids in a 1: 3 planar sudden expansion. *Journal of Non-Newtonian Fluid Mechanics*, *198*, pp.48-58.

[21] Kockmann, N., Föll, C. and Woias, P., 2003, January. Flow regimes and mass transfer characteristics in static micromixers. In *Microfluidics, BioMEMS, and Medical Microsystems* (Vol. 4982, pp. 319-329). International Society for Optics and Photonics.

[22] Poole, R.J., Alfateh, M. and Gauntlett, A.P., 2013. Bifurcation in a T-channel junction: Effects of aspect ratio and shear-thinning. *Chemical Engineering Science*, *104*, pp.839-848.

[23] Domingues, A.F., Poole, R.J. and Dennis, D.J., 2019. Inertial instabilities in a microfluidic mixing-separating device. *Physics of Fluids*, *31*(7), p.074101.

[24] Taylor, G.I., 1934. The formation of emulsions in definable fields of flow. *Proceedings of the Royal Society of London. Series A, containing papers of a mathematical and physical character*, *146*(858), pp.501-523.

[25] Haward, S.J., Poole, R.J., Alves, M.A., Oliveira, P.J., Goldenfeld, N. and Shen, A.Q., 2016. Tricritical spiral vortex instability in cross-slot flow. *Physical Review E*, *93*(3), p.031101.

[26] Poole, R.J., Alves, M.A. and Oliveira, P.J., 2007. Purely elastic flow asymmetries. *Physical review letters*, *99*(16), p.164503.

[27] Haward, S.J. and McKinley, G.H., 2013. Instabilities in stagnation point flows of polymer solutions. *Physics of Fluids*, *25*(8), p.083104.

[28] Kantsler, V., Segre, E. and Steinberg, V., 2008. Critical dynamics of vesicle stretching transition in elongational flow. *Physical review letters*, *101*(4), p.048101.

[29] Vanapalli, S.A., Ceccio, S.L. and Solomon, M.J., 2006. Universal scaling for polymer chain scission in turbulence. *Proceedings of the National Academy of Sciences*, *103*(45), pp.16660-16665.

[30] Burshtein, N., Zografos, K., Shen, A.Q., Poole, R.J. and Haward, S.J., 2017. Inertioelastic flow instability at a stagnation point. *Physical Review X*, *7*(4), p.041039.

[31] Zografos, K., Burshtein, N., Shen, A.Q., Haward, S.J. and Poole, R.J., 2018. Elastic modifications of an inertial instability in a 3D cross-slot. *Journal of Non-Newtonian Fluid Mechanics*, *262*, pp.12-24.

[32] Galindo-Rosales, F.J., Oliveira, M.S. and Alves, M.A., 2014. Optimized cross-slot microdevices for homogeneous extension. *RSC Advances*, *4*(15), pp.7799-7804.

[33] Balducci, A.G., Tang, J. and Doyle, P.S., 2008. Electrophoretic stretching of DNA molecules in cross-slot nanoslit channels. *Macromolecules*, *41*(24), pp.9914-9918.

[34] Abed, W.M., Domingues, A.F., Poole, R.J. and Dennis, D.J., 2017. Heat transfer enhancement in a cross-slot micro-geometry. *International Journal of Thermal Sciences*, *121*, pp.249-265.

[35] ISO :WHITE, Frank M.; MAJDALANI, Joseph. *Viscous fluid flow*. New York: McGraw-Hill, 2006.

9.0 Appendix

Appendix 1

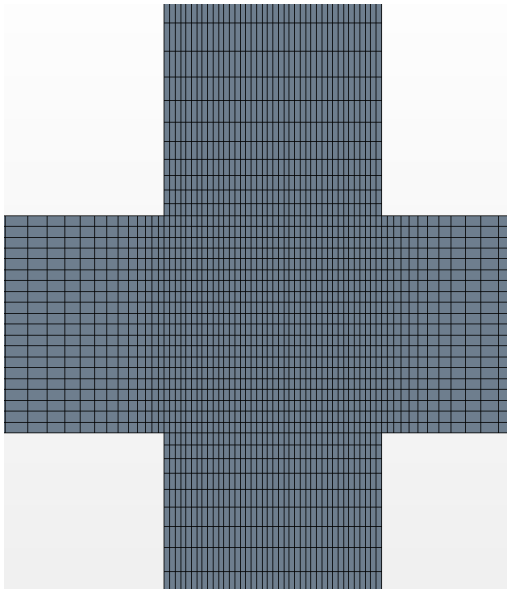

Appendix 2

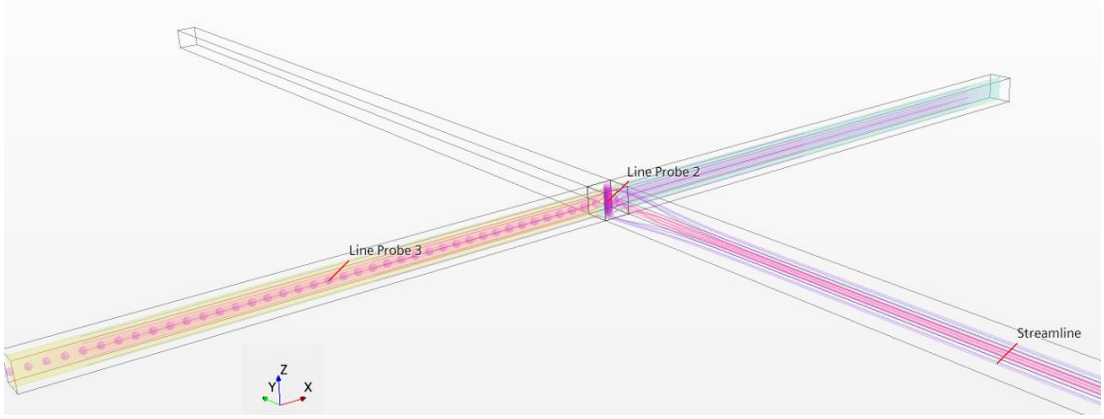

Appendix 3

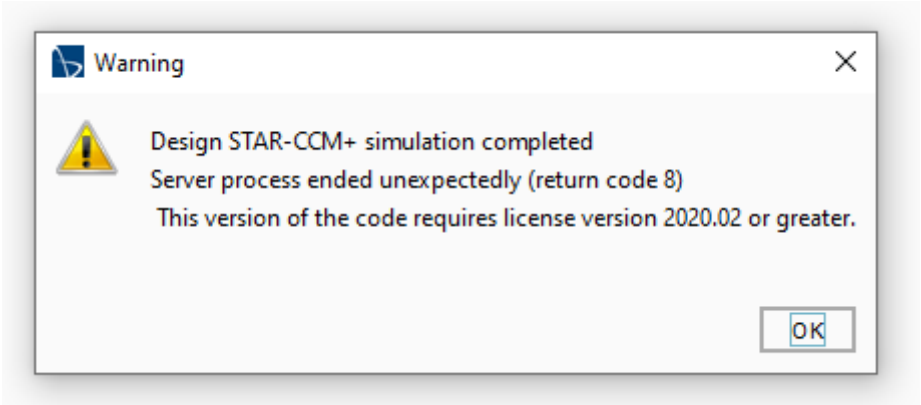

Appendix 4

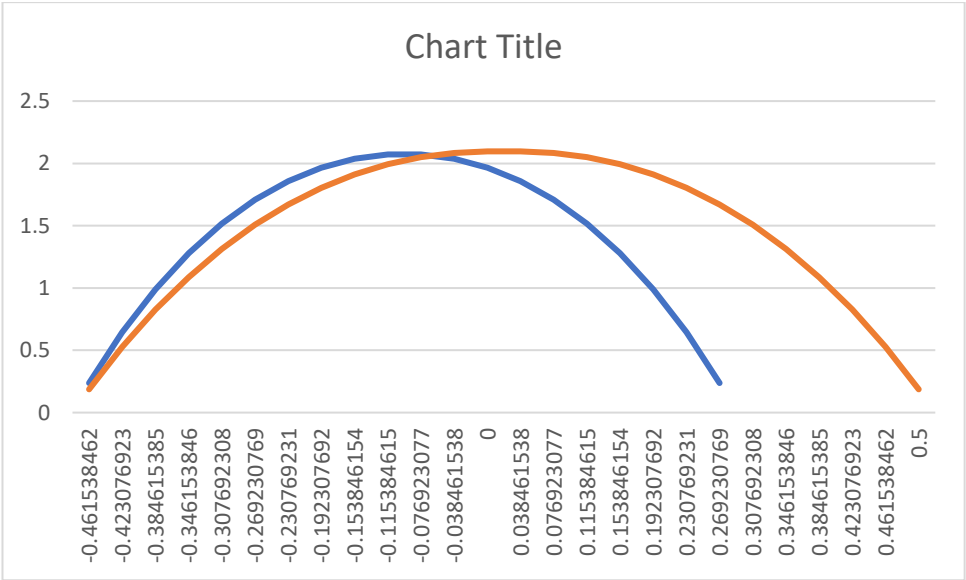

Appendix 5

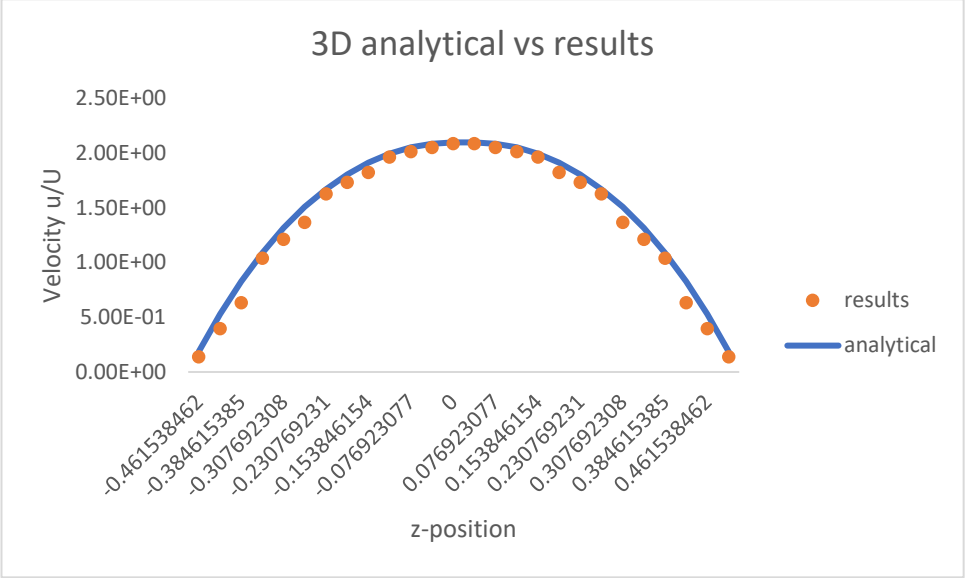

Appendix 6

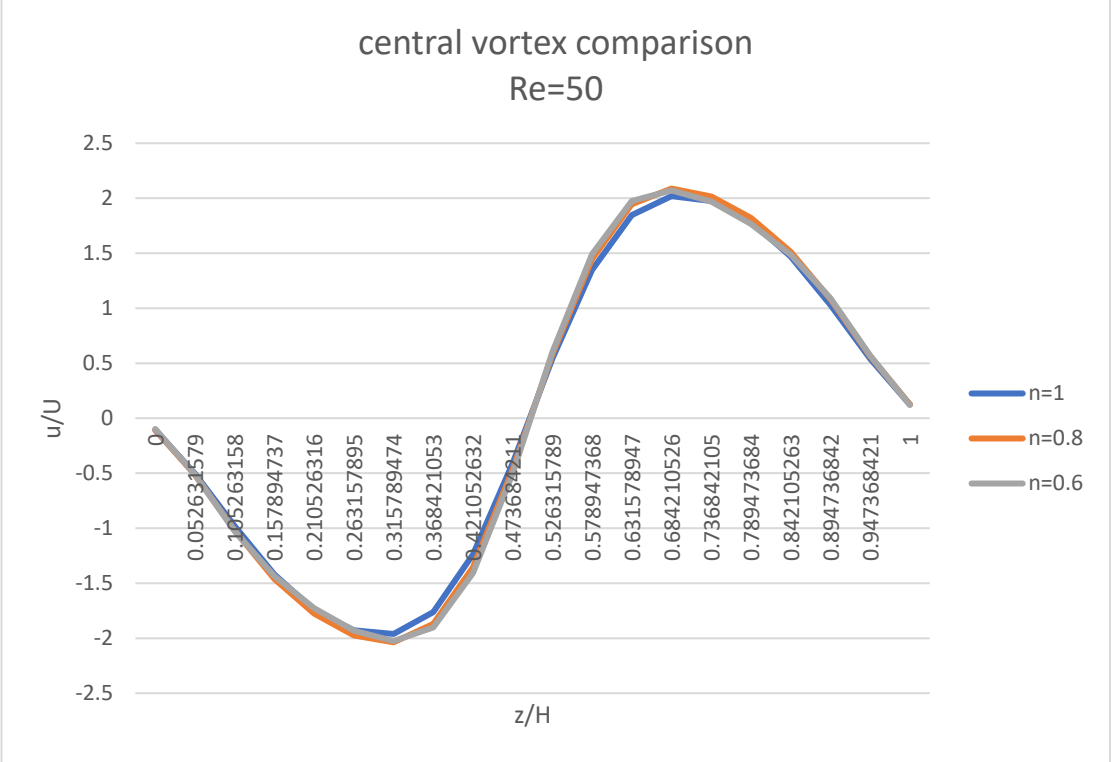

Appendix 7

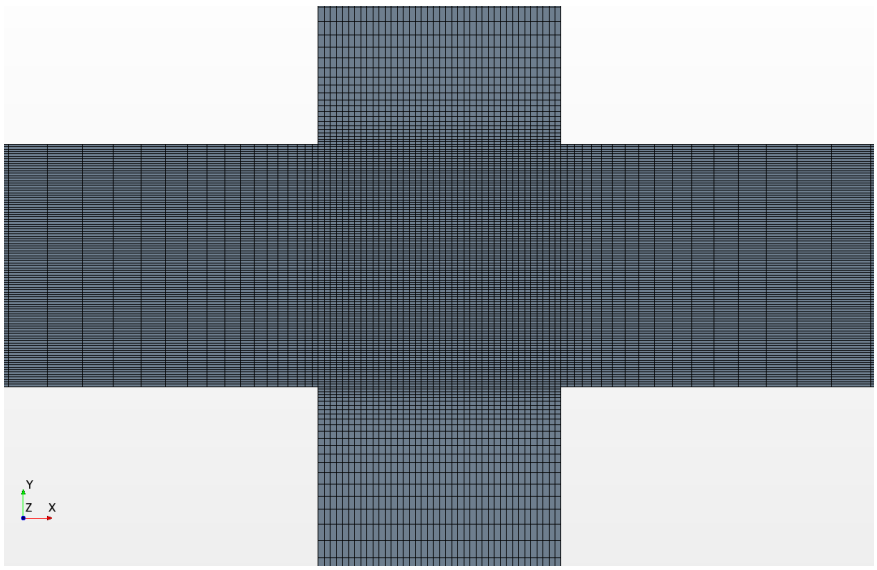
Y
Z X